Journal of Sedimentary Research

Journal of Sedimentary Research, 2019, v. 89, 1–22
Research Article
DOI: http://dx.doi.org/10.2110/jsr.2019.34

SUPERCRITICAL-FLOW DEPOSITS AND THEIR DISTRIBUTION IN A SUBMARINE CHANNEL SYSTEM, MIDDLE EOCENE, AINSA BASIN, SPANISH PYRENEES

PAULINE H. CORNARD AND KEVIN T. PICKERING
Department of Earth Sciences, University College London, Gower Street, London, WC1E 6BT, U.K.
e-mail: pauline.cornard.15@ucl.ac.uk

ABSTRACT: **Studies of supercritical-flow deposits (SFDs) and their spatial distribution in ancient deep-water systems should provide an additional tool to improve the understanding of the flow dynamics during deposition and the architecture of sandbodies. Outcrop recognition of SFDs in ancient deep-marine environments remains poorly documented, although their study dates back to the 1970s. This paper focusses on the criteria for recognizing SFDs and their distribution in three selected depositional environments from an ancient mid-lower slope to a proximal-basin floor setting in the middle Eocene Ainsa Basin, Spanish Pyrenees. From field observations, six facies associations interpreted as related to supercritical flow are defined. These facies associations are grouped in two categories. The first group includes facies associations related to erosional coarse-grained supercritical-flow bedforms related to meter and centimeter-scale scours and backfilling structures interpreted as large-scale cyclic steps or small-scale cyclic steps, respectively. Erosional coarse-grained supercritical bedforms are observed mainly in relatively high-gradient slopes and relatively confined settings. The second group of facies associations are related to depositional fine-grained supercritical-flow bedforms associated with upflow-dipping sandstone lenses, upflow-stacked wavy bedforms, upflow-stacked sigmoidal bedforms, and plane beds, interpreted as unstable and stable antidunes and upper-flow-regime plane beds. Depositional fine-grained supercritical-flow bedforms are observed mainly in relatively unconfined settings such as lower-slope, break-of-slope and proximal basin-floor environments. Two main SFD trends were observed in the Ainsa Basin in: (i) an axial-lateral direction, showing a decrease in SFDs from channel axis to channel margin, and (ii) a longitudinal proximal–distal direction, showing an increase in SFDs from the Gerbe System (mid-slope environment), to the Banastón System (proximal basin-floor environment), to the Ainsa System (lower-slope environment). From this study, two parameters are recognized as likely playing an important role on whether a flow is under supercritical or subcritical conditions: (i) confinement of the sandbodies, and (ii) slope gradient.**

INTRODUCTION

Submarine fans and other deep-water systems can be major oil and gas reservoirs in many sedimentary basins worldwide. In recent years, the increased interest in deep-water reservoirs by the hydrocarbon industry has been a major factor in driving forward a substantial improvement in the understanding of such systems. Sand/mud proportion, grain-size evaluation, bedform architecture, and sedimentary structures all represent criteria used to improve the understanding of deep-water systems. The evaluation of supercritical-flow deposits (SFDs) could provide another useful criterion to understand and constrain the architecture of deep-water systems such as submarine fans.

Flows are considered to be supercritical when the ratio between the flow velocity and thickness exceeds a threshold as defined by the Froude number (Fr). In subaqueous sediment gravity flows (SGFs), the Fr is expressed by the densimetric Fr_d (Yih and Guda 1955; Komar 1971), considering the density contrast between the underflow and the ambient water:

$$Fr_d = \frac{U}{\sqrt{\left(1 - \frac{\rho_{amb}}{\rho_{flow}}\right) gh}} \quad (1)$$

where U is the flow velocity (m s^{-1}), ρ_{flow} and ρ_{amb} are the densities of the flow (kg m^{-3}) and of the ambient water (kg m^{-3}), h is the flow depth (m), and g is the acceleration of gravity (m s^{-2}). In this paper, we refer to the densimetric Fr_d as the Fr. Flows where $Fr > 1$ are said to be supercritical. Flows where $Fr < 1$ are said to be subcritical. SGFs are more likely to have higher Froude numbers than subaerial flows due to a lower density contrast between flow and ambient medium densities. Therefore, SGFs are more likely to form supercritical bedforms.

Sandy submarine fans likely contain abundant evidence for deposition and/or erosion beneath supercritical flows, because it has been postulated that SGFs should be supercritical for slopes $> 0.5°$ (Walker 1967; Komar 1971; Hand et al. 1972; Hand 1974). Supercritical SGFs are believed to be more common in high-gradient submarine canyons and channels in continental slopes, whereas subcritical SGFs are more common in lower-gradient channels and depositional lobes of the continental slope and basin floor (Komar 1971; Mutti and Normark 1987, 1991; Piper and Normark 2001). Many researchers have focused on the recognition criteria for SFDs, including: using numerical modeling for the different flow parameters that create supercritical-flow bedforms (Kostic and Parker 2006; Cartigny et al. 2011; Vellinga et al. 2017); flume-tank experiments (Garcia and Parker 1989; Alexander et al. 2001; Cartigny et al. 2014), or from direct

Published Online: Month 2019
 1527-1404/19/089-000

observations on the seafloor in presently active deep-marine slope and related systems (Fildani et al. 2006; Hughes Clarke et al. 2011, 2012; Covault et al. 2014, 2016; Dorrell et al. 2016; Symons et al. 2016; Normandeau et al. 2016; Hage et al. 2018). An analysis of SFDs in ancient deep-marine environments remains rare (Ito et al. 2014; Postma et al. 2016; Lang et al. 2017a; Ono and Plink-Björklund 2017).

Experimental, theoretical, and observational research suggests that a large range of sedimentary bedforms are produced under varying densimetric Fr. There remains a significant mismatch between this growing body of work and an understanding of how it might map onto field observations in ancient deep-water systems.

The main aim of this paper is to evaluate the various criteria for the recognition of SFDs in an ancient deep-marine setting, the middle Eocene Ainsa Basin, Spanish Pyrenees. After describing and interpreting the various SFDs, we present an analysis of their distribution in different channel and related depositional environments in order to better understand and help constrain the link between depositional setting and SFD distribution. We show that the criteria for SFD distribution could be useful in the future to distinguish and interpret depositional environments.

SUPERCRITICAL-FLOW DEPOSITS (SFDs)

It has long been postulated that deep-water sedimentary bedforms formed under supercritical-flow conditions are commonly associated with hydraulic jumps (e.g., Mutti and Normark 1987; Postma and Cartigny 2014; Postma et al. 2016; and references therein). Hydraulic jumps are produced at the transition from supercritical to subcritical flow. In deep-marine systems, it has been suggested that hydraulic jumps form at a break of slope, e.g., the transition from a confined submarine slope canyon into submarine-fan channels, and also onto an unconfined basin floor (Komar 1971; Mutti and Normark 1987). Numerical modeling suggests that hydraulic jumps can develop spontaneously in slope settings and are therefore not necessarily restricted to the slope break (Mutti and Normark 1987; Fildani et al. 2006; Kostic and Parker 2006; Cartigny et al. 2011). Hydraulic jumps are associated with a wide range of processes such as erosion, flow mixing, and changes in sediment distribution and concentration (Wynn et al. 2002; Cartigny et al. 2011, 2014; Sumner et al. 2013; Macdonald et al. 2011; Hofstra et al. 2015; Symons et al. 2016). In the field, evidence of hydraulic-jump deposits are typically manifest as scours and backfilling structures (Postma et al. 2009, 2016; Ito et al. 2014; Lang et al. 2017a, 2017b).

Under supercritical-flow conditions, a wide variety of bedforms are created (Gilbert 1914; Simons et al. 1965; Allen 1982). Supercritical-flow bedforms formed at low Fr, but still Fr $>$ 1, correspond to the antidune field. Two types of antidunes exist: stable and unstable antidunes (Fr between 0.8 and 1.8; Cartigny et al. 2014). Stable antidunes are bedforms in phase with non-breaking surface waves and with the lowest supercritical Fr (Hand 1974; Cartigny et al. 2014). Most of the time, stable antidunes are observed to migrate upstream, dependent on flow energy and grain size (Gilbert 1914; Kennedy 1961; Middleton 1965; Simons et al. 1965; Hand 1974; Langford and Bracken 1987; Alexander and Fielding 1997; Alexander et al. 2001; Carling and Schvidchenko 2002; Yokokawa et al. 2010). In the rock record, deposits of stable antidunes are characterized by wavy bedforms with sinusoidal stratification (Russell and Arnott 2003; Lang and Winsemann 2013; Slootman et al. 2016), and may resemble hummocky cross-stratification (Walker 1967; Yagishita 1994; Mulder et al. 2009).

Increasing Fr causes antidunes to become unstable such that surface waves start to steepen and break (Hand 1974; Alexander et al. 2001; Cartigny et al. 2014), to form the bedform referred to as an "unstable antidune" (Simons et al. 1965). In outcrop, unstable antidunes have been characterized as gently dipping backsets and foresets with common internal truncations (Hand 1974; Lang and Winsemann 2013; Lang et al. 2017a). The wavelength of preserved antidune deposits range from a few decimeters to several tens of meters (Winsemann et al. 2011; Lang and Winsemann 2013; Lang et al. 2017a).

As Fr increases further, cyclic step and chute-and-pool bedforms develop. They are characterized by the presence of a hydraulic jump.

Cyclic steps are formed at the highest Fr (mean values of the Fr $\sim$ 2.2, Cartigny et al. 2014) and consist of upstream-migrating crescentic-shaped steps. Each step is bounded by regular-spaced hydraulic jumps and comprises a steeply dipping (Fr supercritical) and gently dipping side (Fr subcritical) (Winterwerp et al. 1992; Kostic et al. 2010; Cartigny et al. 2011, 2014). In the rock record, deposits of cyclic steps appear to consist of upflow-dipping backsets, deposited on the stoss side of the bedform and onlap the erosional bed boundary (Kostic and Parker 2006; Cartigny et al. 2011, 2014; Postma and Cartigny 2014; Postma et al. 2014). Scours filled by structureless sand have also been observed and interpreted as cyclic-step deposits in the Monterey Canyon (Fildani et al. 2006; Paull et al. 2010), and in the Squamish Delta, British Columbia (Hage et al. 2018). Due to their long wavelength, cyclic steps (hundreds of meters to kilometers in downstream length) are amongst the most common supercritical-flow bedforms observed on the modern seafloor, with a large range of grain sizes (Fildani et al. 2006; Lamb et al. 2008; Hughes Clarke et al. 2012; Covault et al. 2014, 2016).

The formation of chutes and pools is characterized by the presence of an irregularly spaced hydraulic jump due to their spontaneous occurrence (Winterwerp et al. 1992; Taki and Parker 2005; Kostic et al. 2010; Cartigny et al. 2014). Lately several authors argued that chutes and pools are unstable transitional features between the antidunes and the cyclic steps and they are not preserved in the rock record (Fedele et al. 2016; Massari 2017). Furthermore, chutes and pools need a high sediment aggradation rate to be preserved in the rock record (Lang and Winsemann 2013). Because the issue of preservation of chute and pool deposits is so controversial, we decided to not undertake the description and interpretation of candidate chute and pool bedforms.

A problem is the interpretation of small-wavelength ripples and dunes as having formed as antidunes under supercritical-flow conditions. Pickering and Hiscott (1985), using data from Hand et al. (1972), considered this and noted that antidune wavelengths in turbidites should be $\sim$ 12–14 times the flow depth, so their presence would be imperceptible in most outcrops, i.e., their wavelength under turbidity currents would be in the order of tens to hundreds of meters with bedform amplitudes on the order of tens of centimeters. However, subsequent research suggests that the problem is likely more complex; e.g., Lang et al. (2017a) interpreted aggrading antidunes with wavelengths between 1.2 and 12 m. Postma and Cartigny (2014) argued that bedform wavelength is controlled by the thickness of the dense basal layer for stratified concentrated density flows and by the total flow thickness for turbidity currents (non-stratified flows). From experimental work, Fedele et al. (2016) suggested that ripples can form under subcritical, near-critical, and slightly supercritical flows, with ripples also observed for a range of densimetric Fr of 1.1–1.3 superposed on upstream-migrating antidunes. Caution should be exercised, however, because these experiments involved only saline density currents where the flows were not charged with suspended sediment; i.e., they only reworked the bed and, therefore, may be a special situation in which the morphodynamics might not be the same as for concentrated density flows and turbidity currents. In flume experiments, in a study of the grain-size controls on near-bed density stratification by Tilston et al. (2015), they observed ripple cross-lamination formed under depth-averaged supercritical-flow conditions. Yang et al. (2017, their fig. 1) have described centimeter-scale siltstone to fine-grained sandstone ripples, including climbing ripples, as antidunes and chute-and-pool structures, but this appears to be unsubstantiated by any published theoretical and/or experimental data. In the absence of reliable contrary knowledge for the formation of ripple cross-lamination, in this study we consider ripples

formed under subcritical-flow conditions during deceleration of a sediment-laden flow.

METHODOLOGY

This study involved seven months of fieldwork undertaken in the Ainsa Basin, with 25 detailed sedimentary logs through different submarine-fan and related environments (channel-axis, channel-margin, and levee–overbank settings). In this manuscript, the terminology and definitions we use for the various types of SGFs and their deposits are those of Pickering and Hiscott (2016). For each sedimentary log, the bed thickness, grain size, sedimentary structures, and facies (facies classification scheme of Pickering et al. 1986, modified in Pickering and Hiscott 2016) were recorded. Paleoflow was obtained by measuring the orientation of various sole structures (flute casts, groove casts), current ripples, and clast imbrication. Because outcrops are rarely parallel to paleoflow, we consider sandy bedforms, linked to supercritical flow, with differences between paleoflow and the outcrop photograph generally $< 10°$ but in some cases up to $\sim 20°$.

More than 7,500 beds were measured and analyzed in order to evaluate the distribution of SFDs in the mid-, lower-slope, and proximal basin-floor environments. From the various criteria used to recognize SFDs, such as supercritical-flow bedforms (cyclic steps and antidunes) and other sedimentary structures (backset, planar-parallel lamination), each discrete flow event or deposit was interpreted as completely or partially deposited under supercritical or subcritical flow conditions. The thickness of each part of a bed, or entire bed, interpreted as deposited under supercritical or subcritical conditions was recorded and tabulated. In this analysis, the percentage of supercritical or subcritical flow deposits was calculated for each sedimentary log. The percentage of SFDs was calculated only on the sandstone beds; mudstone intervals have not been taken into account in the calculation, inasmuch as mudstones are considered deposited under subcritical-flow conditions.

Research in the Ainsa Basin has led to a large database of sedimentology, stratigraphy, architectural elements, and structures of the sandbodies (submarine fans and related deposits). This extensive database makes the Ainsa Basin an ideal natural laboratory in which to analyze SFDs and their distribution. Each detailed sedimentary log was measured in sandbodies already interpreted in terms of their depositional environments (from proximal to distal and lateral directions). These environmental interpretations can be found in Pickering and Bayliss (2009) and Pickering and Cantalejo (2015), and references therein. In this paper, our descriptions and interpretations of SFDs are presented in the context of the channel and related environments previously interpreted (above). We should emphasize here that we do not use the percentage of SFDs to interpret channel environments, but only to characterize (hydrodynamically) such environments that have been recognized on other criteria, i.e., there is no circular reasoning in our environmental interpretations.

Due to the lack of observed sedimentary structures and insufficient criteria to recognize SFDs in mass-transport complexes (MTCs) and cohesive-flow deposits (such as debrites), only relatively more dilute SGFs, such as concentrated density flows, also commonly referred to as high-density turbidity currents, and turbidity currents are considered in this study (terminology in Pickering and Hiscott 2016).

GEOLOGICAL SETTING

The middle Eocene Ainsa Basin, south-central Spanish Pyrenees (Fig. 1A), originated as a foreland basin that became a thrust-top (piggyback) basin when it was incorporated into the Gavarnie thrust sheet during the Pyrenean orogeny (e.g., Muñoz 1992; Muñoz et al. 2013). The eastern and western margins of the basin are defined by the Mediano and Boltaña anticlines, which separate the Tremp–Graus Basin (fluvio-deltaic and shallow marine) to the east and the Jaca Basin (submarine lobes and related deposits, including basin floor) to the west. The middle Eocene stratigraphy of the Ainsa Basin comprises submarine fans and related deposits packaged into two groups, the Lower and Upper Hecho Group (Fig. 1B) (Pickering and Cantalejo 2015 and references therein). They accumulated essentially in upper- to mid-bathyal depths of $\sim$ 400–600 m (based on micropaleontological study by Pickering and Corregidor 2005).

This study focusses on selected, representative, parts of various submarine-fan and related deposits in three deep-marine systems in the Ainsa Basin (Fig. 1B): the Gerbe System (mid-slope environment—the youngest system of the Lower Hecho Group), the Banastón System (proximal basin-floor environment—the oldest system of the Upper Hecho Group) and the Ainsa System (lower-slope–base-of-slope environment—middle Upper Hecho Group). The Lower Hecho Group is more structurally deformed than the Upper Hecho Group, and shows locally intense folding, shearing, and thrusting (Pickering and Bayliss 2009). This difference in the deformation has been linked to the emplacement of the so-called Lower-Thrust Sheets (Larra–Boltaña thrust sheet) during the latest Ypresian, interpreted as the transition from a foreland basin *sensu stricto* to a thrust-top basin (Remacha et al. 2003; Pickering and Bayliss 2009). The degree of tectonic deformation in the Hecho Group decreases upwards until the deep-marine Guaso System. This progressive decrease in tectonic deformation upward through the Ainsa Basin demonstrates an important synsedimentary tectonic influence on deposition in the deep-marine basin.

Gerbe System (899 Beds Logged)

The Gerbe System is stratigraphically located between the Arro and the Banastón systems in the Lower Hecho Group. It has been interpreted as a submarine canyon slope-channel system (Clark and Pickering 1996). The Gerbe sandy fans were deposited in mid-slope canyon to lower-slope erosional channel settings (Millington and Clark 1995; Pickering and Bayliss 2009). Millington and Clark (1995) recognized a change in depositional style, which they interpreted as showing an upward change from a sheet system in a base-of-slope canyon during the deposition of the Arro System, to a submarine-canyon channel during the deposition of the Gerbe System. The Gerbe System consists of two sandy fans named the Gerbe I Fan (older) and Gerbe II Fan (younger). Detailed sedimentary logs were produced for the mid-slope environment of the Gerbe System (Fig. 2: Gerbe I Fan: Log 1; Gerbe II Fan: Logs 2 and 3).

Banastón System (5,450 Beds Logged)

The Banastón System directly overlies the Gerbe System and is the oldest system deposited in the Upper Hecho Group. The system comprises six sandy fans, designated form oldest to youngest, Banastón I to Banastón VI, respectively. These sandy fans show a transitional depositional style from lower-slope channel infill in the eastern part of the Ainsa Basin, to a more proximal basin-floor and fan lateral-margin and levee–overbank environments in the northwest and northeast of the basin (Bayliss and Pickering 2015). Sedimentary logs were produced in the northwest part of the Ainsa Basin, i.e., in proximal basin-floor fan environments (Fig. 2: Banastón I Fan: Logs 4, 5, and 6; Banastón II Fan: Logs 7, 8, and 9; Banastón III Fan: Logs 10 and 11; Banastón IV Fan: Logs 12 and 13; Banastón V Fan: Logs 14 and 15; Banastón VI Fan: Logs 16, 17, and 18).

The Banastón I Fan lower-slope channel–canyon infill is mapped as having deposits restricted between the Mediano (in the east) and the Añisclo anticlines in the west. The Banastón II and III fans are mapped as showing no significant changes in thickness over the Añisclo Anticline; therefore, it is assumed that this structure had temporarily stopped growing or that sediment supply exceeded the rate of growing seafloor relief (see fig. 13 in Bayliss and Pickering 2015), leading to a decrease in confinement of the sandbodies from Banastón I to III fans. However, we

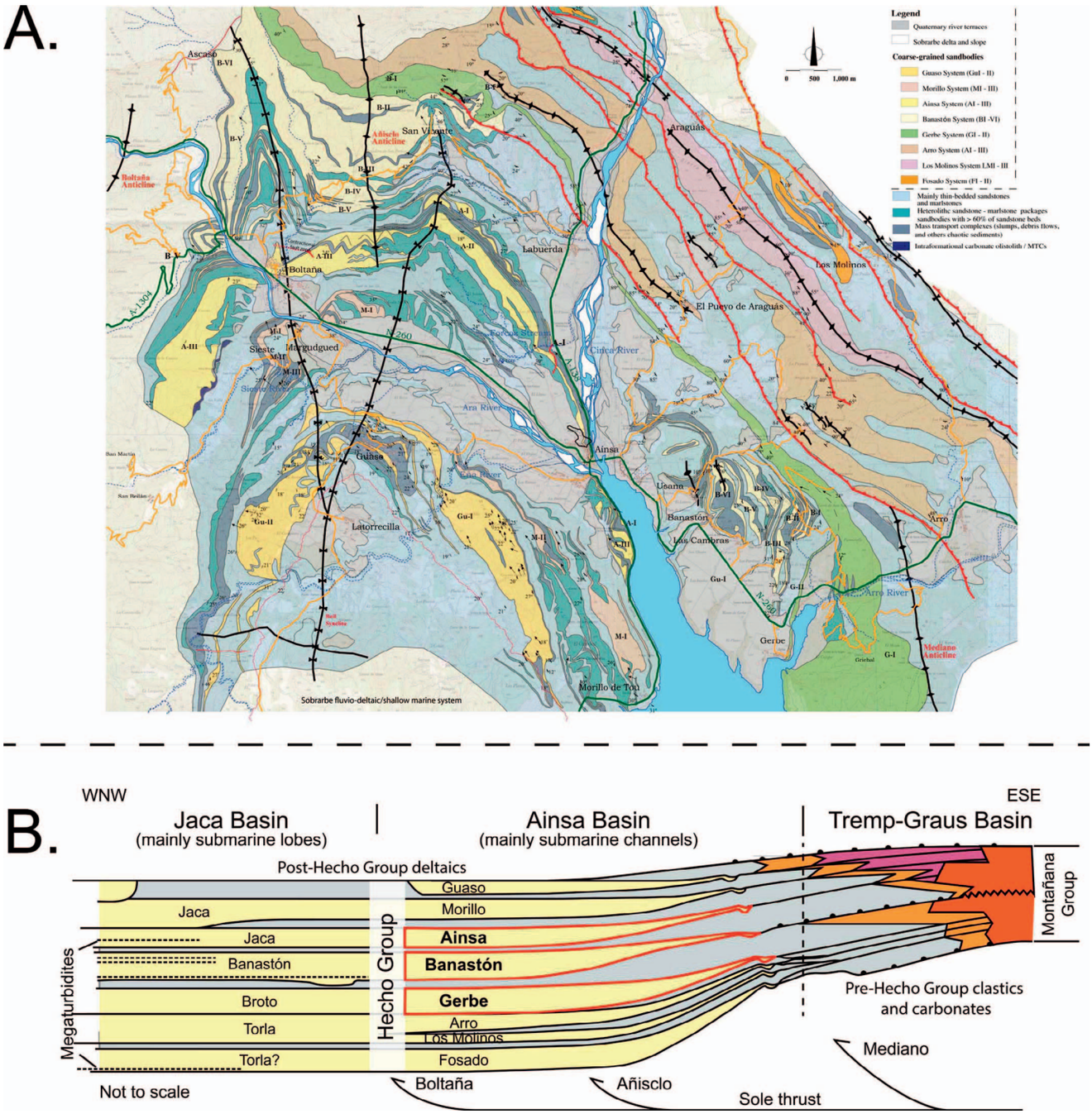

FIG. 1.—**A)** Geological map of the Ainsa Basin; from Pickering and Bayliss (2009). **B)** Schematic summary stratigraphy of the Hecho and Montañana groups in the South Pyrenean foreland Tremp–Graus, Ainsa, and Jaca basins (modified from Scotchman et al. 2015). The Montañana Group is middle Eocene fluvio-deltaic and associated shallow-marine sediments and is not part of this study. The three studied systems are underlined in red (Gerbe, Banastón, and Ainsa systems) in the Ainsa Basin.

emphasize that the presence of the thickest MTDs (up to ~ 20 m) at the base of Banastón III probably enhanced local topographic confinement. It appears that during the final stages, or after the deposition of the Banastón III Fan, the Añisclo Anticline was reactivated as the Banastón IV, V, and VI fans are located to the west of the Añisclo Anticline (Bayliss and Pickering 2015). From mapping, a progressive decrease in the confinement of the Banastón IV, V, and VI fans is observed, without significant synsedimentary tectonic activity of the Añisclo Anticline, or the sediment accumulation rate of these three fans exceeded (drowned) any structural growth of the anticline (Bayliss and Pickering 2015).

Ainsa System (2,391 Beds Logged)

The Ainsa System stratigraphically overlies the Banastón System. The Ainsa System comprises three sandy fans, interpreted as structurally confined, lower-slope submarine fans with erosional–depositional channels

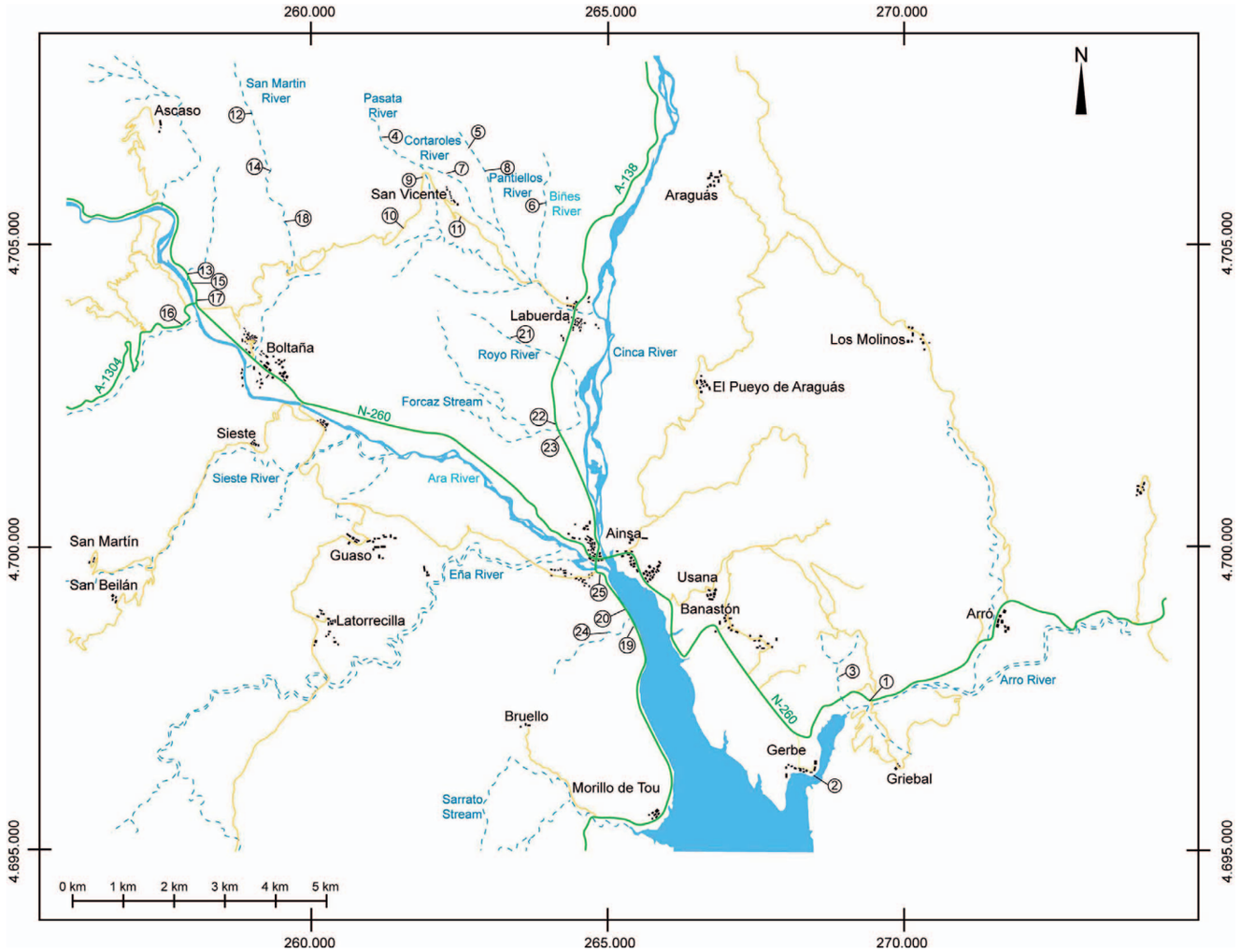

FIG. 2.—Geographic location of the detailed sedimentary sections logged as part of this study.

and proximal basin-floor environments (Pickering and Corregidor 2005; Pickering et al. 2015). The fans show decreasing confinement from the Ainsa I to III fans, likely due to a period of relative tectonic quiescence in the basin. The Ainsa I Fan shows more lateral confinement compared with the Ainsa II and III fans, due mainly to the presence of type I MTCs (Pickering and Corregidor 2005) which created topography (ponded accommodation).

Apart from the spectacular cliff outcrops around Ainsa, the Ainsa II Fan has less accessible exposures for detailed sedimentological observations than the other Ainsa fans, so only the Ainsa I and III fans were incorporated into this study, with detailed sedimentary logs made in the lower-slope environment of the Ainsa System (Fig. 2: Ainsa I Fan (channel 1): Logs 19 and 20; Ainsa I Fan (channel 2): Logs 21, 22, and 23; Ainsa III Fan: Logs 24 and 25).

FACIES ASSOCIATION RELATED TO SFDs

In the Ainsa Basin, a wide range of supercritical-flow bedforms and associated sedimentary structures are observed in the deep-marine deposits. From observations, six different facies associations linked to SFDs are presented. Within the six facies associations, two categories of bedforms are recognized: (i) erosional coarse-grained bedforms of FA1a and FA1b, and (ii) depositional fine-grained bedforms of FAs 2a, 2b, 3, and 4. Bedforms are always described parallel to the main paleoflow.

Erosional Coarse-Grained Supercritical-Flow Bedforms

FA1a: Meter-Scale Scours and Backfilling Structures.—Description.—Scours are from 2–5 m long and 1–2 m deep and are asymmetric with a high angle (15–20°) in the upstream side and low angle (5–10°) in the downstream side, filled with pebbly sandstones and graded stratified sandstones. The pebbly sandstones at the bases of the scours show considerable thickness variation, between 20 and 70 cm. Representative examples of these scour infills are shown in Figure 3A and 3B. Figure 3A shows an infill dominated by pebbly sandstones (Facies Group A1 of Pickering and Hiscott 2016) and graded stratified sandstones (Facies Group B2 of Pickering and Hiscott 2016). These deposits show convex-upward gently-dipping backset stratification underlain by subrounded to well-rounded pebbles (size range 3–15 cm) and angular mudclasts with some imbrications showing upflow-inclined *a–b* planes. Graded stratified sandstones, observed at the top of scours, show convex-upward backset lamination that may be underlain by, and incorporate, mudclasts (1–5 cm) with a progressive transition to planar-parallel lamination at the top. Figure 3B shows a scour infill dominated by graded pebbly sandstones observed

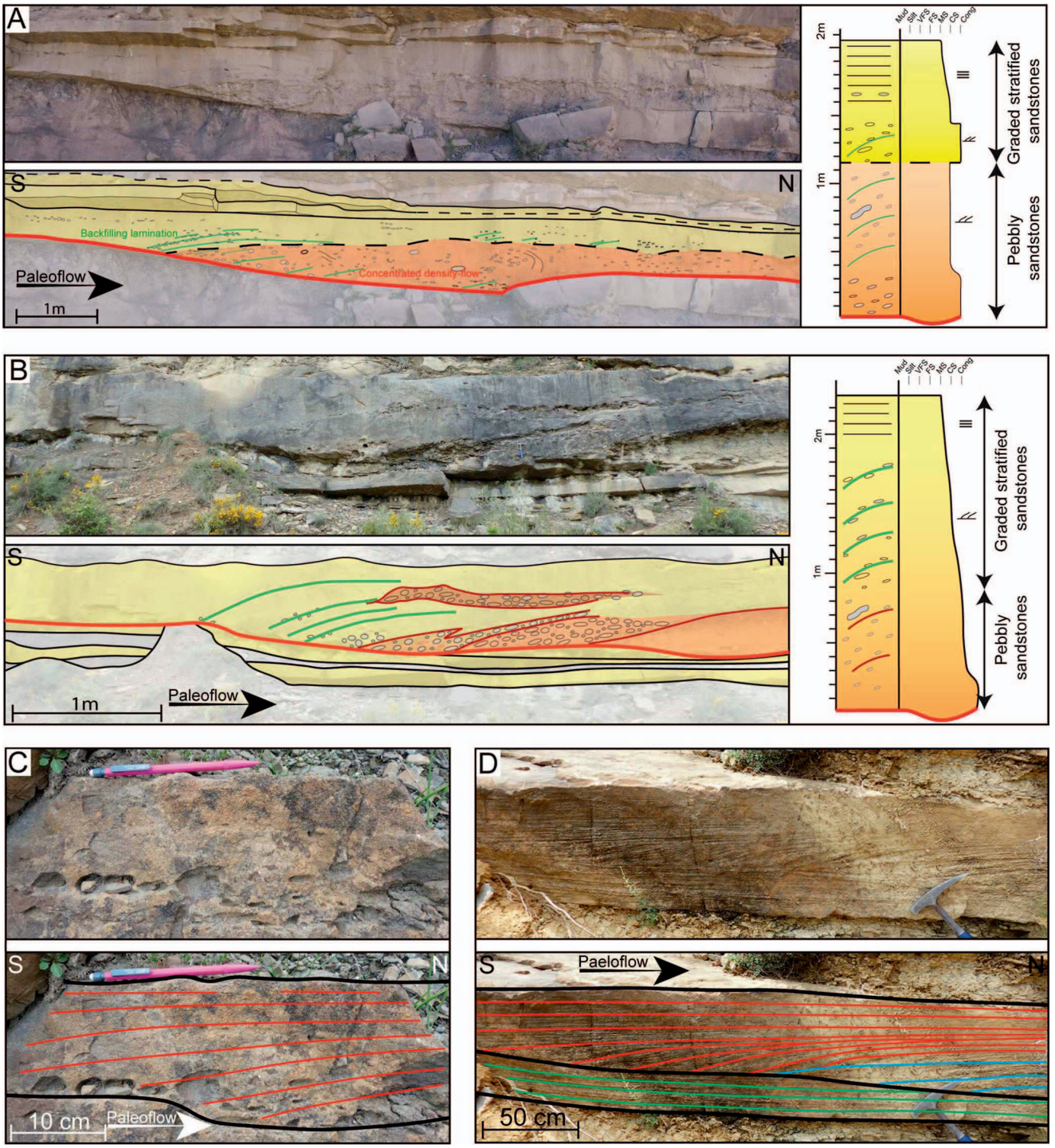

FIG. 3.—**A)** FA1a meter-scale scours and backfilling structures. Outcrop in the Ainsa Quarry, basal part of Ainsa I Fan (lower-slope channel-axis environments). Spoon-shaped scour filled by discrete SGF deposits. At the base of the scour, concentrated density-flow deposits showing convex-backset lamination underlain by pebbles and mudclasts. Above this, there is an abrupt transition to turbidites, also showing convex-backset lamination. A progressive transition to parallel and foreset lamination occurs at the top of the deposits. **B)** FA1a meter-scale scours and backfilling structures. Outcrop in the Ainsa Quarry, Ainsa I Fan (lower-slope channel-axis environments). Asymmetric scour filled by a single SGF event. Scour surface outlined by a red thick line to show the erosion surface. At the base of the scour, there are concentrated density-flow deposits with convex-backset lamination. There is an upward change from concentrated density-flow deposits to turbidites with a progressive reduction in sand grain size and a reduction in the proportion of outsize clasts. Convex-backset lamination observed at the base of the turbidites is underlain by pebbles and mudclasts. At the top of the turbidites, there is a progressive transition from convex-backset lamination to parallel and foreset lamination. **C)** FA1b centimeter-scale scour-and-backfilling structures. Outcrop along Barranco Royo in the Ainsa I Fan (lower-slope channel-axis environments). Centimeter-scale scour filled by medium-bedded, medium-grained sandy turbidites. Backset lamination underlain by centimeter-scale mudclasts is present at the base of the deposit with a progressive transition to parallel lamination at the top. **D)** FA1b centimeter-scale scour-and-backfilling structures. Outcrop in the Banastón III Fan (proximal basin-floor channel-axis environments) near San-Miguel church, San Vicente village. Centimeter-scale scour is filled by several SGF events. Turbidites showing two sets of backset lamination with varying dips from low-angle long backset lamination (in blue), to higher-angle convex-backset lamination (in red).

at the base of the scour and graded stratified sandstones above (Facies Group A2 and B2 of Pickering and Hiscott 2016). Convex-backset lamination in the pebbly sandstones is underlain by pebbles and angular mudclasts. At the transition between the deposits, there is a reduction in grain size and in the amount of pebbles and mudclasts. Only the convex-upward backset lamination observed at the base of graded stratified sandstones are underlain by pebbles and mudclasts.

Interpretation.—Pebbly sandstones and graded stratified sandstones are interpreted as concentrated density-flow deposits and turbidites, respectively. The asymmetric scour shape associated with convex-upward backset lamination suggests the presence of a hydraulic jump, with the upstream migration of the hydraulic jump eroding the upstream side and depositing on the downstream side (Cartigny et al. 2014; Postma et al. 2016; Lang et al. 2017a; Ono and Plink-Björklund 2017). The convex-upward backset lamination can be interpreted to preserve the migration of hydraulic jumps in an upflow direction (Jopling and Richardson 1966; Macdonald et al. 2009; Ito et al. 2014). In Figure 3A, the scour infill shows an abrupt vertical transition from a concentrated density-flow deposit and an immediately overlying turbidite. Convex-upward backset lamination is consistent with the concentrated density flow and turbidity current having undergone a hydraulic jump. It is difficult to discern how many flow events infill the scour. One hypothesis involves infill of a scour by one discrete flow event undergoing a transition between a concentrated density flow and a turbidity current while going through a hydraulic jump. Due to the initial flow undergoing a hydraulic jump, there was rapid deposition of most of the bedload, in turn leading to a decrease of flow density and concentration, then leading to a flow transformation from a concentrated density flow into a more dilute SGF (turbidity current), all within the zone of a hydraulic jump (Weirich 1988). This transition must have been quite rapid, because the physical transition between the two deposits is abrupt. An alternative hypothesis is that the infill of the scour was from two discrete flow events—first a concentrated density flow undergoing a hydraulic jump and depositing its bedload, followed by a turbidity current that also underwent a hydraulic jump. The absence of a scour at the base of the upper turbidite leads us to prefer the first hypothesis. Pebbles and angular mudclasts underlying the convex-backset lamination suggest the action of erosive concentrated density flows and turbidity currents associated with increased turbulence due to hydraulic jumps (Komar 1971; Garcia and Parker 1989; Garcia 1993; Ito et al. 2014). Furthermore, erosion could have happened before the hydraulic jump, due to increased shear stresses associated with faster and thinner supercritical flow on the lee side of the bedform, also incorporating angular mudclasts into the flow (Vellinga et al. 2017). Planar-parallel lamination observed in the deposits infilling the uppermost part of the scours can be interpreted as the T_b division of the Bouma sequence, covering the hydraulic-jump deposits (convex-upward backset lamination) interpreted here as the T_a division of the Bouma sequence (Postma et al. 2009).

In Figure 3B, the transition between a concentrated-density-flow deposit and the overlying turbidite can be explained by a progressive transition between a concentrated density flow into a turbidity current while the flow is undergoing the hydraulic jump (Weirich 1988), as explained in the first hypothesis for the first example of a scour infill (above).

These meter-scale scour-and-fill structures are interpreted as candidate large-scale cyclic-step deposits (Postma et al. 2014, 2016; Lang et al. 2017a; Ono and Plink-Björklund 2017). The presence of angular mudclasts underlying and within the convex-backset lamination suggests erosional hydraulic-jump zones, where intense turbulence with upward flow migration triggers liquefaction and probably rip-up of the unconsolidated substratum (Komar 1971; Lennon and Hill 2006; Postma et al. 2009, 2014; Ito et al. 2014; Lang et al. 2017a). Their presence might argue for a train of scours where the mudclasts are incorporated into a highly erosive flow to be rapidly deposited in successive (down-flow) scours, i.e., the mudclasts have not come from the scour in which they sit but rather upflow scours and erosion such as might be expected in cyclic steps.

Only isolated scour and backfilling structures have been observed in the Ainsa Basin. Limited exposure is likely the best explanation for this observation. We suspect that with larger outcrops in a downflow direction trains of scours might well have been observed. In other outcrop studies, where scour-and-fills are interpreted as cyclic-step deposits, only isolated scour-and-backfilling structures have been observed (Postma et al. 2016; Lang et al. 2017a; Ono and Björklund 2017) due to the poor preservation of these bedforms, which depend on both the magnitude of the SGFs and net sediment aggradation rates (Hage et al. 2018).

FA1a is the first type of erosional coarse-grained bedform and was observed in the channel axis of the Gerbe (I and II), Banastón I, and Ainsa I fans, suggesting that large-scale cyclic steps are present mainly in relatively high slope gradients (mid-slope environment) and in confined settings in lower-slope and proximal basin-floor environments.

FA1b: Centimeter-Scale Scours and Backfilling Structures.— Description.—The main difference between the FA1a and FA1b is the scale of the scours. Scours of FA1b are characteristically 30–80 cm long and 20–50 cm deep and show an asymmetric shape. These spoon-shaped scours are filled by thick- to thin-bedded, fine- to coarse-grained sandstones. As in FA1a, two types of scour infills are observed. In the first case, sandstone beds show a progressive transition from convex-backset lamination to longer and less inclined backsets, to planar-parallel lamination at the top of the deposits (Fig. 3C). In the second case, different angles are observed in a succession of stacked deposits showing convex-backset lamination (Fig. 3D). A break in the angle of convex-backset lamination is seen from long inclined backset lamination to high-angle convex-backset lamination. Each set of backsets is normally graded with an abrupt transition from fine- to coarse-grained sandstone between the set of backset lamination. No planar lamination was observed between two sets of convex-backset lamination, but planar-parallel lamination is observed at the top of the bedforms. In some cases, the convex-backset lamination is underlain by angular mudclasts.

Interpretation.—As in FA1a, the asymmetric shape associated with convex-backset lamination of the scour implies the occurrence of a hydraulic jump (Cartigny et al. 2014; Postma et al. 2016; Lang et al. 2017a; Ono and Plink-Björklund 2017). The presence of convex-upward lamination suggests an upstream migration of a hydraulic jump in the flow where the backset lamination is formed downstream of the upstream-migrating hydraulic jump (Jopling and Richardson 1966; Macdonald et al. 2009; Ito et al. 2014; Postma et al. 2014). Both types of scour infill show a progressive decrease in grain size, and these deposits are interpreted as turbidites. In the first type, the scour is infilled by one discrete turbidity current, and the progressive transition from convex-backset lamination to long-backset and planar-parallel lamination is probably explained by the reduction of average grain size, flow velocity, and bedload discharge (Massari and Parea 1990; Massari 1996). In the second case, the scour is filled by different turbidity-current deposits created during several hydraulic jumps. When the flow undergoes a hydraulic jump, it erodes the convex-backset lamination of the underlying deposits, thereby explaining the backset lamination with varying internal angles. The lack of planar-parallel lamination at the top of the initial deposit can be explained by a reworking of planar-parallel lamination by a subsequent flow event into convex-backset lamination while the flow undergoes a hydraulic jump.

These centimeter-scale scour-and-fill structures are interpreted as candidate small-scale cyclic steps. The dimension of cyclic steps depends on the flow discharge, flow depth, slope, grain size, and thickness of the dense basal layer (Postma and Cartigny 2014), therefore, the wavelength of cyclic steps can form at any length from tens of meters to several kilometers (Kostic and Parker 2006; Lamb et al. 2008; Spinewine et al.

2009; Hughes Clarke 2016). In the case of FA1b, infills are mainly turbidites, whereas infills of FA1a are both concentrated density-flow deposits and turbidites; therefore, the type of SGF might have had an influence on the scale of the scour. Structures of FA1b appear very similar to the high-angle cross-stratified sandstone infilling a small-scale scour, forming a downflow-lengthening set, as described by Arnott and Al-Muffi (2017). However, the paleoflow direction is 180° to that inferred in the Ainsa Basin, therefore leading us to a very different interpretation for bedform formation.

FA1b is part of the erosional coarse-grained bedform category and is observed in all three studied systems (Gerbe, Banastón, and Ainsa fans), but is dominant in coarse-grained sand and confined environments such as the channel axis of the Gerbe, Banastón I, and Ainsa I fans.

Depositional Fine-Grained Supercritical-Flow Bedforms

FA2a: Upflow Dipping Sandstone Lenses.—Description.—FA2a is characterized by upflow-dipping lenticular sandstone beds. Lenses are thin- to medium-bedded, medium- to fine-grained sandstone. Lenses vary from 50 cm to 4 m long. Lenses can occur as a train of solitary lenticular bedforms (Fig. 4A), or as vertically stacked lenses in an upflow direction (Fig. 4B, C). Within an individual lens, the inclination of the lamination varies widely, from convex upward in the upstream side to foreset dipping in the downstream parts. Generally, a structureless mudstone layer is observed at the top of the train of the solitary lenses. In stacked lenses, truncation and scour surfaces are observed at a decimeter scale. Most of the lamination is observed at the top of the lenses, whereas strata in the lower part are structureless. At outcrop, lenses can have a concave (Fig. 4B) or convex-up (Fig. 4A, C) shape.

Interpretation.—Upflow-dipping lenticular bedforms with variable internal architecture (backset to foreset) are interpreted as antidune deposits (e.g., Cheel 1990; Alexander et al. 2001; Cartigny et al. 2014; Ono and Plink-Björklund 2017). Based on bedform descriptions in flume experiments by Cartigny et al. (2014), FA2a is interpreted as candidate unstable antidune deposits. The multiple truncations observed are interpreted as having been produced by the upstream migration of a surge, eroding and forming the lenticular shape. Depending on how far the surge migrates, sediments are deposited on the stoss side of the lens, forming backset lamination, then due to a pulse in the flow, the surge is flushed downstream, reworking the top of the lens into foreset lamination (Cartigny et al. 2014). Depending on the amount of sand supplied to the depositional surface, this facies association occurs either as solitary lenses or upflow-stacked centimeter-scale lenses. The structureless mud cap observed at the top of the train of solitary lenses is likely explained by the high mud content. One hypothesis could be that the solitary lenses are mainly formed within the basal layer of the SGF. The main body of the SGF could have had a high concentration of suspended mud, creating a mud drape at the top of the solitary lenses, also suggesting that the flow may have been stratified. Upflow-dipping sandstone lenses are commonly observed in the channel axis of the Banastón and Ainsa sandbodies and are part of the fine-grained depositional bedform category. One good example of trains of solitary lenses is observed in the channel axis of the Gerbe II Fan.

FA2b: Upflow-Stacked Wavy Bedforms.—Description.—FA2b is characterized by medium- to thick-bedded, medium- to coarse-grained sandstone showing wavy bedforms. Their wavelength is irregular and varies from 70 to 380 cm. Depending on the outcrops, wavy bedforms show varying amplitudes, from high-amplitude waveforms (10–20 cm from the bottom of the scour to the top of the bedform crest) (Fig. 5A, B) to low-amplitude waveforms (5–10 cm), thereby making them hard to observe in many outcrops. Troughs at the top of the bedform have an asymmetric shape with a steep lee side and a gently inclined stoss side and are filled by structureless mudstones or sandstones. The internal architecture exhibits a large variation in the dip of laminae from convex-backset, subhorizontal to foreset lamination. These types of lamination are developed at the tops of the bedforms. The bottom part of the bedform is characterized by a structureless deposit or backset lamination.

Interpretation.—As observed in FA2a, the presence of convex-backset and foreset lamination suggests that deposition was under supercritical-flow conditions (Alexander et al. 2001; Spinewine et al. 2009; Cartigny et al. 2014). The scale, wavelength, and internal structures are consistent with the interpretation as unstable-antidune deposits (Cartigny et al. 2014). Unstable-antidune deposits of FA2a and FA2b have different shape and thickness. These differences can be explained by the strength of the upstream-migrating surge. The surge in FA2a has to be strong enough to erode and scour the sediment located upstream to create a lenticular shape to the bed. In FA2b, the upstream-migrating surge is weaker than for the unstable antidunes of FA2a, and produces troughs only at the tops of the bedforms. Structureless mudstone or sandstone infilling a trough is interpreted to represent deposition of the remaining part of the flow or a later flow.

Upflow-stacked wavy bedforms are observed mainly in the channel axis of Banastón and Ainsa fans.

FA3: Upflow-Stacked Sigmoidal Bedforms.—Description.—FA3 is characterized by meter-scale sigmoidal bedforms. The term sigmoidal is used to define the shape of a bedform that has an "S" form. Upflow-stacked sigmoidal beds are medium- to thick-bedded, medium- to coarse-grained sandstone 2–6 m long (Fig. 6A, B, C). Sigmoidal bedforms show characteristic variation from structureless sandstone in the lower part of a bed to normally graded low-angle convex-backset lamination at the top of a bed on the upstream sides of bedforms. The downstream side of the bedform shows subhorizontal lamination and foreset low-angle lamination.

Interpretation.—As in FA2a and FA2b, the presence of backset lamination and convex-upward lamination suggests deposition under supercritical-flow conditions (Alexander et al. 2001; Spinewine et al. 2009; Cartigny et al. 2014). Upflow-stacked bedforms suggest upflow bedform migration. Upflow-stacked bedforms together with convex-backset, foreset, and subhorizontal lamination are interpreted as deposition from upstream-migrating stable antidunes (Lang et al. 2017a). Upflow-stacked sigmoidal bedforms are seen mainly in channel-axis and off-axis sites in the Banastón and Ainsa sandy fans and are part of the fine-grained depositional bedforms category.

FA4: Plane Bed.—Description.—Plane bed occurs as very thin- to thick-bedded, very fine- to medium-grained sandstone that shows planar-parallel lamination (Fig. 6D, E). Beds show a sharp base with paleoflow indicators as flutes or grooves. Planar-parallel lamination may occur at the bottom and/or top of a bed. Where they occur in the lower part of a bed, they are typically underlain by mudclasts and pebbles (< 1 cm). In most cases, ripple cross-lamination overlies the plane beds. Due to poor exposure, it is difficult to follow plane beds for lateral distances greater than approximately 10 m.

Banded layers in sandstone are observed in the middle of a bed and are commonly associated with structureless beds. This structure is characterized by centimeter-scale normally graded (and in some cases inverse-graded) parallel (planar) layers of coarse-grained sediment.

Observations of planar-parallel lamination in the Ainsa System in Well L2 core from the Ainsa Basin were undertaken (see well location in Pickering et al. 2015). No mineral segregation was observed. However, lamination is visible because of grain-size segregation, with the coarsest grains forming the laminae. In some cases, it is possible to observe grain imbrication in these laminae (upflow-dipping *a–b* planes). Each lamina is separated by the structureless finest grain size.

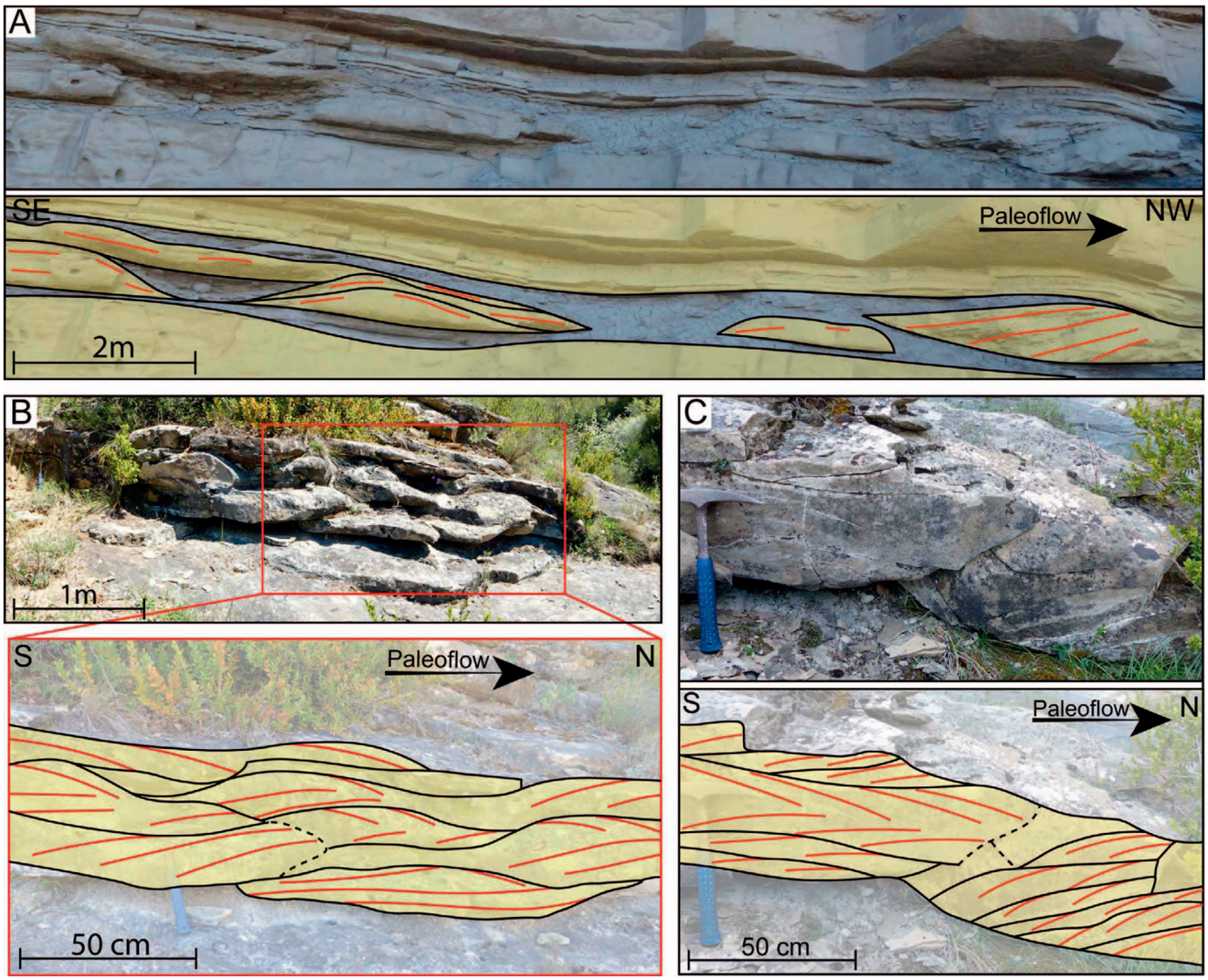

FIG. 4.—**A)** FA2a, showing individual lenticular bedforms. Outcrop in the Gerbe II Fan (mid-slope channel-axis environments) near Gerbe village. Trains of symmetric lenticular bedforms with a structureless mud cap are observed. Each bedform is 1–6 m long and 30–50 cm thick. Some lenses are stacked, which can be interpreted as successive discrete SGF deposits. The lens observed at the right of the picture is interpreted as FA1a representing a part of a large-scale cyclic step. **B)** FA2a related to upflow-dipping centimeter-scale lenticular beds. Outcrop in the Ainsa III Fan (lower-slope channel-axis environments) along Rio Buchosa. In this case, lenses with a concave-up shape can reach 1 m long. They show a large variability in the dip of lamination from backset, sub-planar parallel to foreset lamination. Many truncation surfaces are also observed. **C)** FA2a related to upflow-dipping centimeter-scale lenticular beds. Outcrop in the Ainsa III Fan (lower-slope channel-axis environments) along the Rio Buchosa. Stacked lenses with a convex-up shape, varies between 10 and 30 cm thick, normally graded, medium- to fine-grained sandstones. Most of the lenses are structureless at the base and show backset lamination at the top; some lenses show foreset lamination at the top with truncation surfaces.

Interpretation.—We interpret the plane-bed deposits described above as having formed under upper-flow-regime (UFR) conditions (supercritical flow). There is considerable disagreement amongst researchers over UFR plane-bed formation, i.e., if UFR plane beds are formed under supercritical or subcritical conditions. UFR plane beds can be found in three supercritical-flow bedforms: the very low-amplitude bedforms (in-phase bed), in plane bed under slow aggradation rates (Allen 1984; Paola et al. 1989; Cheel 1990) and on the stoss sides of cyclic-step bedforms (Postma and Cartigny 2014). In most cases, the parallel lamination can be interpreted as the Bouma T_b division in turbidites (cf. traction carpet of Hiscott 1994 and Postma et al. 2009). Skipper (1971) and Walker (1965) proposed that UFR plane beds observed in the T_b division of the Bouma sequence formed under supercritical-flow conditions. Fielding (2006) asserted that plane beds with a grain size from very fine- to medium-grained sandstone formed under supercritical-flow conditions (UFR). Tilston et al. (2015) suggest that formation of plane beds may be related to how sediment is distributed in the flow. Throughout the Ainsa Basin, the widespread presence of spaced parallel (banded layers) stratification in sandy deposits is used as evidence for traction under supercritical turbulent currents (cf. Hiscott and Middleton 1979; Hiscott 1994; Postma et al. 2009).

Observation of planar-parallel lamination in Well A2 core show grain-size segregation and grain imbrication interpreted as a shear fabric created during flow (laminar sheared layer), possibly criteria for supercritical-flow conditions (cf. Paola et al. 1989; Sumner et al. 2008).

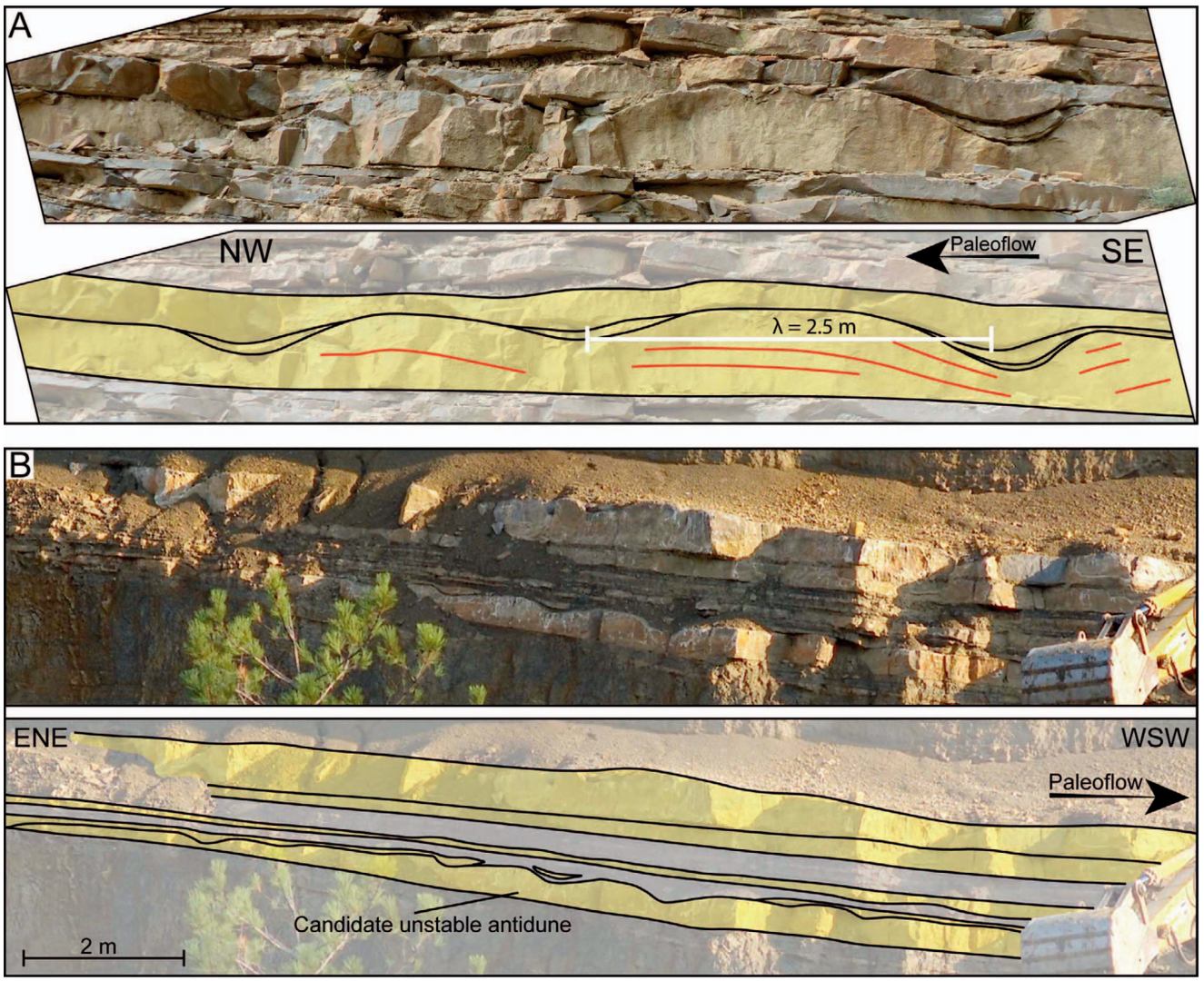

FIG. 5.—**A)** FA2b upflow-stacked wavy bedforms. Outcrop in the Banastón VI Fan (proximal basin-floor channel-axis environments). This bedform is characterized by a high-amplitude waveform with a wavelength of ~ 2.5 m. The base of the bedform is structureless and the top shows a large variation in the dip of lamination. Troughs at the top of the bedform are filled by structureless mudstones and sandstones. **B)** FA2b upflow-stacked wavy bedforms, Banastón V Fan in the Usana Quarry (lower-slope environment). Bedform wavelength is irregular, between ~ 1.5 to 2 m. Bedform is lensing towards ESE. Troughs at the top of the bedform are also filled by structureless mudstones and sandstones.

Ripple cross-lamination is observed at the tops of upper-plane beds, showing flow deceleration to produce bedforms interpreted as the T_c division of the Bouma sequence formed by tractional reworking of fine-grained sediment (Sumner et al. 2008). As in many previous studies, we note the absence of dunes between the upper-plane beds and the ripple cross-lamination (for a discussion of this issue and possible explanations, see section 1.5.7 in Pickering and Hiscott 2016).

The interpretation of upper-plane bed in terms of facies association requires some discussion, because they could be observed in many of the facies associations described above (FA1a, FA1b, FA2a, FA2b, or FA3). Plane beds observed over lateral distances $> \sim 10$ m can be interpreted as UFR plane beds. Where the lateral exposure is more limited ($< \sim 10$ m), it is difficult, if not impossible, to interpret plane beds as FA4 because they could be part of another supercritical-flow bedform described above (e.g., long-wavelength antidunes, FA2a, FA2b, and FA3, or on the stoss sides of cyclic steps, FA1a).

FA4 was observed in many types of depositional environments, from channel axis to channel levee–overbank in all three studied systems (the Gerbe, Banastón, and Ainsa sandy fans).

DISTRIBUTION OF SUPERCRITICAL-FLOW DEPOSITS

Gerbe System (Mid-Slope Environment)

Interpretations of depositional environments of the Gerbe System and constituent fans are based on the following papers: Millington and Clark (1995), Clark and Pickering (1996), and Pickering and Bayliss (2009).

Gerbe I Fan.—In the Gerbe I Fan, a detailed sedimentary log was compiled in channel-axis deposits. The lower part of the Gerbe I Fan consists mainly of medium- to thick-bedded, structureless, concentrated density-flow deposits with pebble to coarse-grade sandstones. Supercrit-

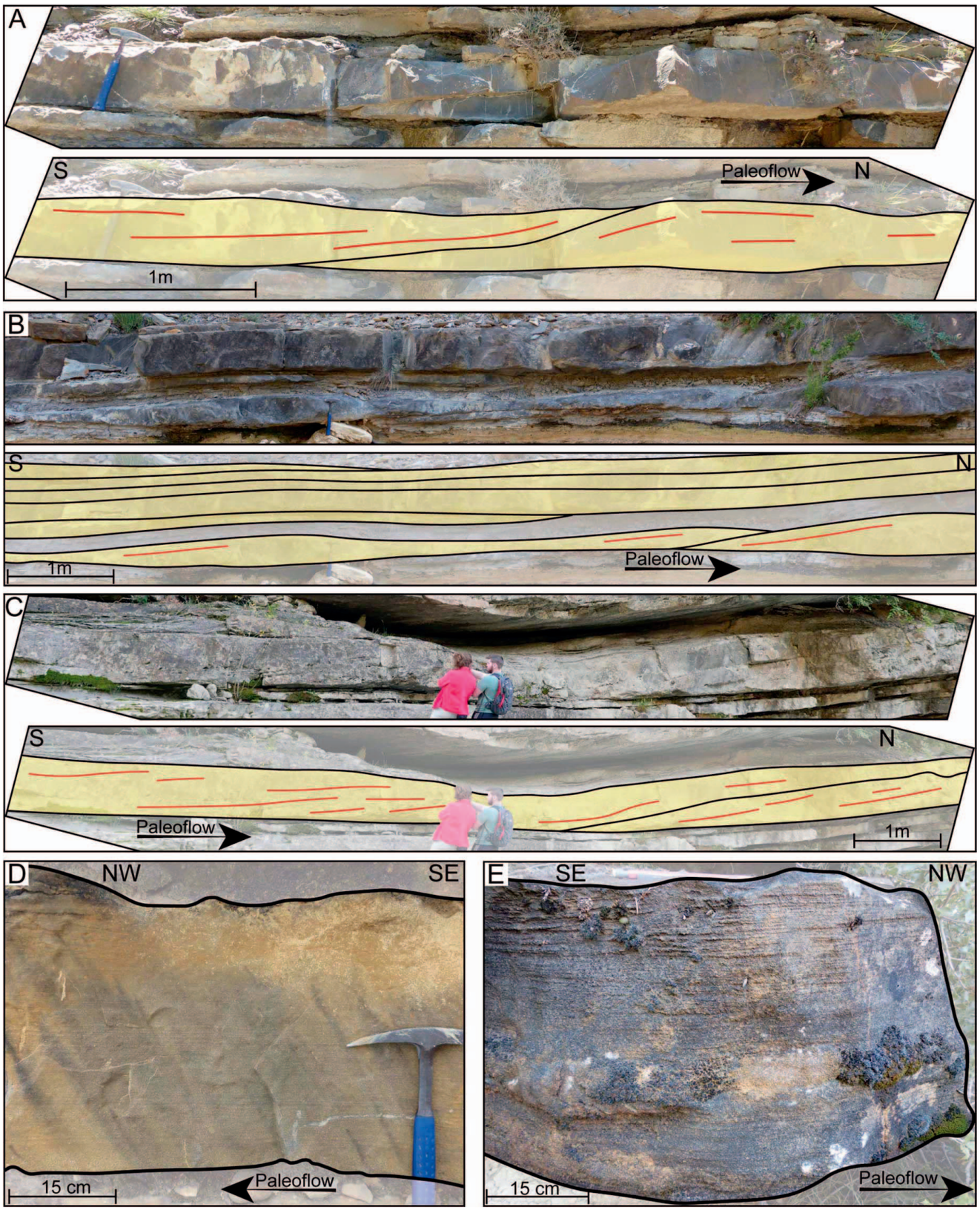
A
S
Paleoflow
N
1m
B
S
N
1m
Paleoflow
C
S
N
Paleoflow
1m
D
NW
SE
15 cm
Paleoflow
E
SE
NW
15 cm
Paleoflow

ical-flow bedforms were observed only in the upper and finer-grained parts of the sedimentary log in the sandy fan deposits. 35% of the Gerbe I Fan total sandstone thickness (Table 1, Log 1) can be interpreted to have been deposited under supercritical-flow conditions.

Gerbe II Fan.—In the Gerbe II Fan, four detailed sedimentary logs were measured (three logs in channel-axis and one log in channel levee–overbank deposits). The three sedimentary logs in channel-axis deposits are along an upflow–downflow transect (Log A is the more proximal and log C more distal—summarized in Table 1, Log 2A, B, and C). Most of the candidate supercritical-flow bedforms recognized in the channel axis are candidate unstable antidunes (FA2a) and cyclic steps (FA1a and FA1b). Log B shows good examples of scour-and-backfilling structures and individual (solitary) lenticular bedforms, interpreted as candidate cyclic steps (FA1a and FA1b) and unstable antidune (FA2a), respectively (Fig. 7). Outcrop limitations mean that the sedimentary logs were made with horizontal separations of 20–50 m. These three closely spaced logs provide an opportunity to check the degree of accuracy of the method used. Because the sedimentary logs are spaced equal to the bedform length, very similar percentages of SDFs were expected in these logs. The three logs show a similar proportion of sediments deposited under supercritical-flow conditions (Log A, 40%; Log B, 42%; Log C, 33%). Therefore, the error bar is estimated to be on the order of 9% (from 42% to 33%). Supercritical-flow bedforms recognized in the channel levee–overbank are mainly stable-antidune deposits or upper-plane beds. The channel levee–overbank deposits show a proportion of SFDs similar to that of the channel axis, with 32% (Table 1, Log 3).

Banastón System (Proximal-Basin-Floor Environment)

Interpretations of depositional environments for the Banastón System and constituent fans are based on Bayliss and Pickering (2015).

Banastón I Fan.—Three detailed sedimentary logs in the Banastón I Fan (Table 1, Logs 4, 5, and 6) were measured. The channel axis shows a high content of structureless conglomerates and coarse-grained sandstones. At the base of the fan, candidate cyclic steps (FA1a) are observed. The channel axis of the Banastón I Fan contains one of the lowest proportions of SFDs in the Banastón System, with 37% of the logged section. The channel margin is composed mainly of many very fine- to fine-grained sandstones comprising subcritical-flow bedforms such as dunes and ripples, explaining the low proportion of SFDs.

Banastón II Fan.—From the three detailed sedimentary logs in the Banastón II Fan (Table 1, Logs 7, 8, and 9), a decrease is observed in the proportion of SFDs from the channel axis to the channel margin. More supercritical-flow structures such as stable (FA3) and unstable antidunes (FA2a and FA2b) have been observed in the Banastón II Fan than in the Banastón I Fan, explaining the increase of the percentage of SFDs between these two fans.

Banastón III Fan.—From the two detailed sedimentary logs in the Banastón III Fan (Table 1, Logs 10 and 11), no significant changes in the proportion of SDFs are observed between the channel axis (45%) and channel off-axis (38%). Changes in the proportion of SFDs are expected between various depositional environments, e.g., channel-axis and off-axis sites will be associated with SGFs with differences in hydrodynamics (flow density, velocity, and height). Where no significant changes ($> 9\%$) are observed between the channel-axis and channel off-axis environments, we suspect that the detailed sedimentary logs were too close to each other and made in essentially similar sedimentary environments. Channel widths are typically up to several hundred meters, making it difficult to precisely define channel-axis, off-axis, and channel-margin environments.

Banastón IV Fan.—The two sedimentary logs in the Banastón IV Fan are spaced $\sim$ 1,000 m apart (Table 1, Logs 12 and 13). An insignificant decrease in the proportion of SFD is observed from the channel-axis sites (44%) to channel off-axis (36%) sites (Fig. 8). Even if the percentages of SFDs is somewhat similar between channel-axis and channel off-axis sites, making it difficult to characterize different channel environments, it is still possible to observe a variation in the type of supercritical-flow bedforms (high or low Fr) between channel environments. Several erosive supercritical-flow structures (high Fr) were observed in the channel axis, e.g., small-scale cyclic-step deposits (FA1b). In contrast, supercritical-flow bedforms with a lower Froude number (but $Fr > 1$) are more common in channel off-axis sites than in channel-axis sites (e.g., FA3 and FA4).

Banastón V Fan.—As in the Banastón III Fan, the Banastón V Fan shows no significant change in the percentage of SFDs from channel-axis sites (39%) to channel off-axis sites (34%) (Table 1, Logs 14 and 15) (Fig. 8). The channel-axis environment contains erosional supercritical-flow bedforms, e.g., candidate cyclic steps (FA1a and FA1b). Many candidate unstable and stable antidunes (FA2a, FA2b, and FA3) and upper-plane bed (FA4) deposits containing a high proportion of medium- and coarse-grained sandstone were recorded in channel off-axis environments. The high proportion of erosional structures in channel-axis environments can be explained by the presence of several hydraulic jumps creating the scours with a rapid reduction in flow turbulence immediately following a hydraulic jump, leading to deposition of most of the bedload (high proportion of Facies Class A of Pickering and Hiscott 2016).

Banastón VI Fan.—From the three sedimentary logs in the Banastón VI Fan (Table 1, Logs 16, 17, and 18), a decrease in the proportion of SFDs is observed from the channel-axis to the channel off-axis and channel-margin sites (Fig. 8). The channel axis in the Banastón VI Fan is characterized by many supercritical-flow bedforms, such as candidate stable (FA3) and unstable antidunes (FA2a and FA2b) and upper-plane beds (FA4), dominated by medium- to fine-grained sandstones. The Banastón VI Fan shows the highest percentage of SFDs of all the Banastón fans. The Banastón VI Fan is considered to be more depositional rather than erosional (and with less sediment bypass), compared with the other

←

FIG. 6.—**A)** FA3 upflow-stacked sigmoidal bedforms. Outcrop in the Ainsa II Fan (lower-slope channel-axis environments) along Barranco Forcaz. This upflow-stacked sigmoidal bedform is thick-bedded, coarse- to medium-grained sandstone, with a structureless base and a large variability in the dip in the lamination from backset, sub-planar parallel to foreset lamination at the top. **B)** FA3 upflow-stacked sigmoidal bedforms. Outcrop in the Banastón II Fan (proximal basin-floor channel off-axis environment). The bedform located at the base of the outcrop, is medium-bedded, medium- to fine-grained sandstone, with a structureless base and a progressive transition to backset bedding at the top. **C)** FA3 upflow-stacked sigmoidal bedforms. Outcrop in the Morillo II Fan (lower-slope environment). Although the Morillo System is not documented in detail in this study, it shows very good examples of supercritical-flow bedforms. This upflow-stacked bedform is thick-bedded, coarse- to medium-grained sandstone, showing mainly backset lamination from the base to the top of the bedform. Ripple cross lamination is observed at the top. **D)** FA4 plane beds. Outcrop in Banastón V Fan (proximal basin-floor channel-axis environments), road section, Boltaña. This medium-bedded, medium- to fine-grained sandstone shows planar-parallel lamination throughout the bed. **E)** FA4 plane beds. Outcrop in the Banastón III Fan (proximal basin-floor channel-axis environments). Medium-bedded, medium- to fine-grained sandstones with planar-parallel lamination throughout most of the beds but with ripple lamination at the top. In this example, planar-parallel lamination is easier to observe due to the presence of a shear fabric.

TABLE 1.—Percentage of the total thickness calculated for each sedimentary log of the sandstone and mudstone (silt is included in sandstone percentages), bed thickness (very thin beds, 1–3 cm; thin beds, 3–10 cm; medium beds, 10–30 cm; thick beds, 30–100 cm; very thick beds, > 100 cm; Pickering and Hiscott 2016), Facies Classes (Facies Class A, gravels, muddy gravels, gravelly muds and pebbly sand; Facies Class B, sands; Facies Class C, sand–mud couplets and muddy sands; Facies Class D, silts, silty muds and silt–mud couplets; Facies Class E, muds and clays; facies classification scheme of Pickering and Hiscott 2016), grain size and proportion of SFDs (the percentage of mudstone is not taken into account in the calculation of proportion of SFDs). The sedimentary logs are in different fan environments in an across-fan (lateral) direction (channel axis to the channel margin and levee–overbank) and in a proximal-to-distal direction, from a mid-slope environment (Gerbe System), proximal-basin floor environment (Banastón System), and lower-slope environment (Ainsa System).

Depositional environments	GERBE SYSTEM (MID-SLOPE)					BANASTÓN SYSTEM (PROXIMAL BASIN-FLOOR)					
Log numbers	1	2			3	4	5	6	7	8	9
Systems	**Gerbe I** Channel axis (80 beds)	**Gerbe II** Channel axis (698 beds) A	B	C	**Gerbe II** Channel levées-overbank (121 beds)	**Banastón I** Channel axis (228 beds)	**Banastón I** Channel off-axis (160 beds)	**Banastón I** Channel margin (460 beds)	**Banastón II** Channel axis (230 beds)	**Banastón II** Channel off-axis (209 beds)	**Banastón II** Channel margin (183 beds)
Sandstone	54%	73%	55%	62%	35%	53%	42%	41%	54%	51%	36%
Mudstone	46%	27%	45%	38%	65%	47%	58%	59%	46%	49%	64%
Very-thin beds	25%	34%	36%	36%	42%	21%	18%	49%	30%	32%	34%
Thin beds	36%	38%	37%	39%	53%	28%	41%	45%	23%	46%	48%
Medium beds	19%	20%	24%	17%	5%	29%	34%	6%	22%	20%	17%
Thick beds	16%	8%	3%	8%	0%	17%	7%	0%	24%	2%	1%
Very-thick beds	4%	0%	0%	0%	0%	5%	0%	0%	1%	0%	0%
Facies A	32%	0%	0%	0%	0%	22%	3%	0%	4%	3%	0%
Facies B	6%	35%	26%	31%	4%	10%	7%	4%	15%	11%	17%
Facies C	17%	29%	27%	30%	27%	22%	31%	29%	35%	33%	18%
Facies D	3%	3%	1%	0%	4%	2%	1%	8%	0%	5%	1%
Facies E	42%	33%	45%	38%	65%	44%	58%	59%	46%	48%	64%
Silt proportion	3%	3%	1%	0%	4%	1%	1%	8%	0%	5%	1%
Very-fine sandstone	6%	4%	4%	4%	8%	1%	4%	8%	3%	4%	2%
Fine sandstone	3%	14%	19%	18%	14%	9%	15%	17%	9%	17%	7%
Medium sandstone	4%	27%	21%	19%	8%	14%	18%	8%	26%	19%	15%
Coarse sandstone	11%	20%	10%	20%	1%	19%	3%	1%	10%	4%	10%
Conglomerates	28%	0%	0%	2%	0%	8%	0%	0%	5%	1%	0%
Sandstone deposited under supercritical conditions	35%	40%	42%	33%	32%	37%	31%	26%	58%	40%	31%

TABLE 1.—*Continued.*

Depositional environments	BANASTÓN SYSTEM (PROXIMAL BASIN-FLOOR)								
Log numbers	10	11	12	13	14	15	16	17	18
Systems	**Banastón III** Channel axis (345 beds)	**Banastón III** Channel off-axis (264 beds)	**Banastón IV** Channel axis (746 beds)	**Banastón IV** Channel off-axis (345 beds)	**Banastón V** Channel axis (983 beds)	**Banastón V** Channel off-axis (378 beds)	**Banastón VI** Channel axis (336 beds)	**Banastón VI** Channel off-axis (390 beds)	**Banastón VI** Channel margin (192 beds)
Sandstone	42%	29%	47%	53%	60%	66%	78%	52%	33%
Mudstone	58%	71%	53%	47%	40%	34%	22%	48%	67%
Very thin beds	44%	51%	23%	20%	24%	24%	20%	31%	51%
Thin beds	39%	34%	28%	43%	28%	45%	37%	43%	45%
Medium beds	17%	15%	33%	28%	31%	25%	29%	19%	4%
Thick beds	0%	0%	16%	9%	16%	5%	12%	7%	0%
Very thick beds	0%	0%	0%	0%	1%	1%	2%	0%	0%
Facies A	0%	0%	2%	8%	12%	18%	1%	14%	0%
Facies B	11%	8%	14%	19%	14%	13%	41%	17%	8%
Facies C	30%	18%	36%	27%	41%	36%	35%	29%	22%
Facies D	1%	3%	1%	1%	0%	1%	1%	0%	3%
Facies E	58%	71%	47%	45%	33%	32%	22%	40%	67%
Silt proportion	1%	3%	1%	1%	0%	1%	1%	0%	3%
Very fine sandstone	3%	2%	2%	3%	2%	4%	3%	1%	8%
Fine sandstone	18%	11%	13%	10%	8%	14%	20%	8%	16%
Medium sandstone	16%	11%	26%	18%	21%	19%	33%	18%	5%
Coarse sandstone	3%	2%	11%	16%	34%	14%	20%	22%	0%
Conglomerates	0%	0%	0%	0%	2%	6%	1%	2%	0%
Sandstone deposited under supercritical conditions	45%	38%	44%	36%	39%	34%	53%	30%	30%

Depositional environments	AINSA SYSTEM (LOWER-SLOPE)						
Log numbers	19	20	21	22	23	24	25
Systems	**Ainsa I** – Channel 1 – Channel axis (107 beds)	**Ainsa I** – Channel 1– Channel axis / off-axis (224 beds)	**Ainsa I** – Channel 2 – Channel axis (72 beds)	**Ainsa I** – Channel 2 – Channel off-axis (221 beds)	**Ainsa I** – Channel 2 – Channel margin (183 beds)	**Ainsa III** – Channel axis (327 beds)	**Ainsa III** – Channel off-axis (135 beds)
Sandstone	82%	67%	77%	46%	49%	92%	46%
Mudstone	18%	33%	23%	54%	51%	8%	54%
Very thin beds	8%	45%	12%	41%	70%	59%	51%
Thin beds	26%	21%	27%	37%	22%	28%	25%
Medium beds	32%	22%	38%	20%	8%	10%	13%
Thick beds	30%	12%	23%	2%	0%	2%	11%
Very thick beds	4%	0%	0%	0%	0%	0%	0%
Facies A	11%	7%	7%	6%	3%	0%	6%
Facies B	44%	20%	55%	17%	9%	61%	11%
Facies C	25%	35%	19%	24%	27%	28%	29%
Facies D	2%	5%	0%	4%	13%	3%	1%
Facies E	18%	34%	19%	50%	47%	8%	53%
Silt proportion	2%	2%	0%	3%	14%	4%	1%
Very fine sandstone	1%	4%	0%	3%	9%	14%	5%
Fine sandstone	7%	17%	5%	15%	16%	49%	13%
Medium sandstone	23%	18%	37%	21%	8%	25%	19%
Coarse sandstone	41%	23%	34%	5%	2%	0%	7%
Conglomerates	7%	2%	0%	0%	0%	0%	2%
Sandstone deposited under supercritical conditions	52%	59%	61%	44%	31%	66%	34%

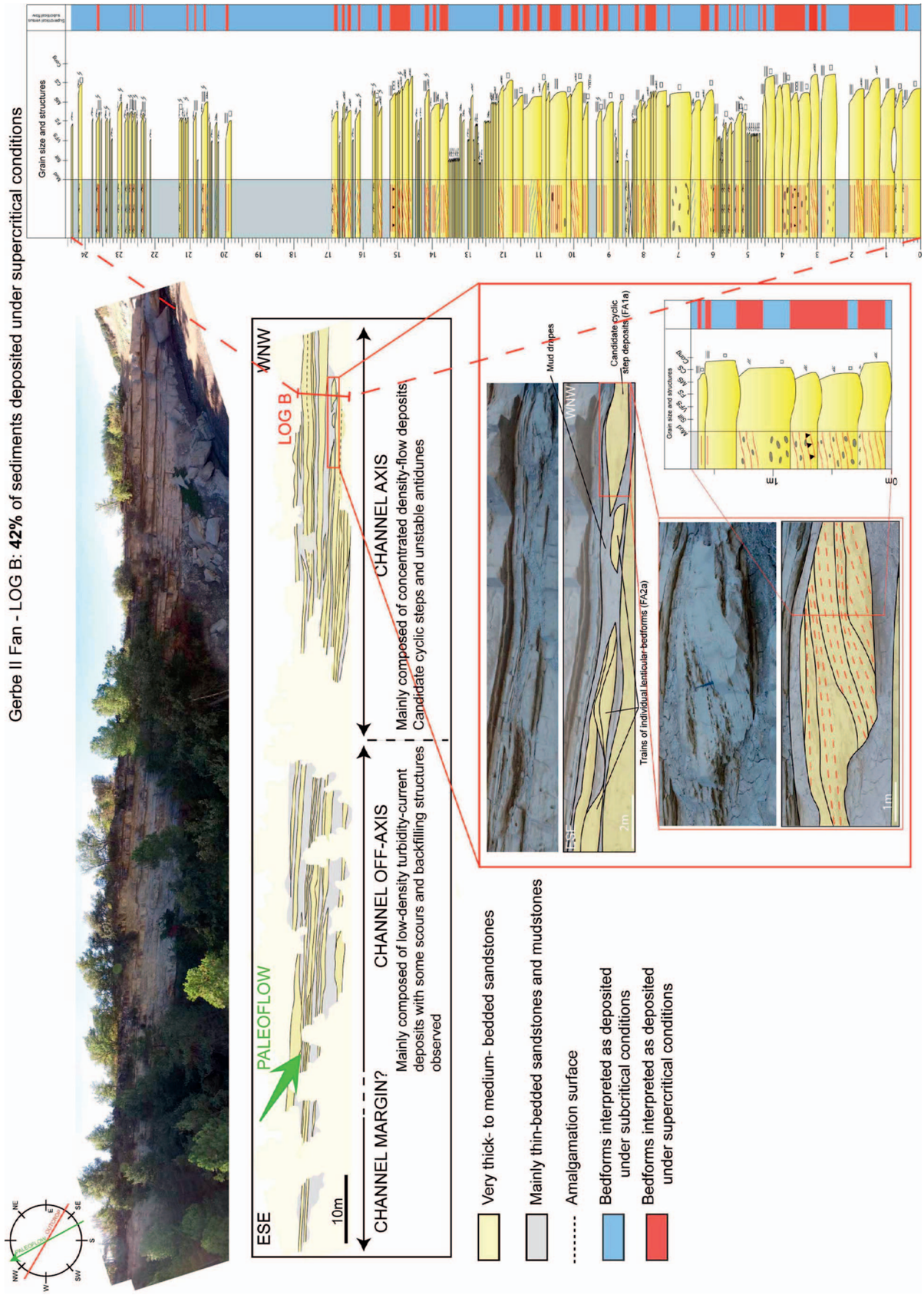

FIG. 7.—Panorama of the Gerbe II cliff where Log B was measured in channel-axis deposits (42% interpreted as SFDs). The outcrop of the channel off-axis was inaccessible, but it is possible to observe a decrease in the sandstone content and in supercritical-flow structures such as scours and backfilling structures and/or lenticular bedforms. The base of the Log 2 shows a good example of candidate large-scale cyclic steps and unstable antidune deposits.

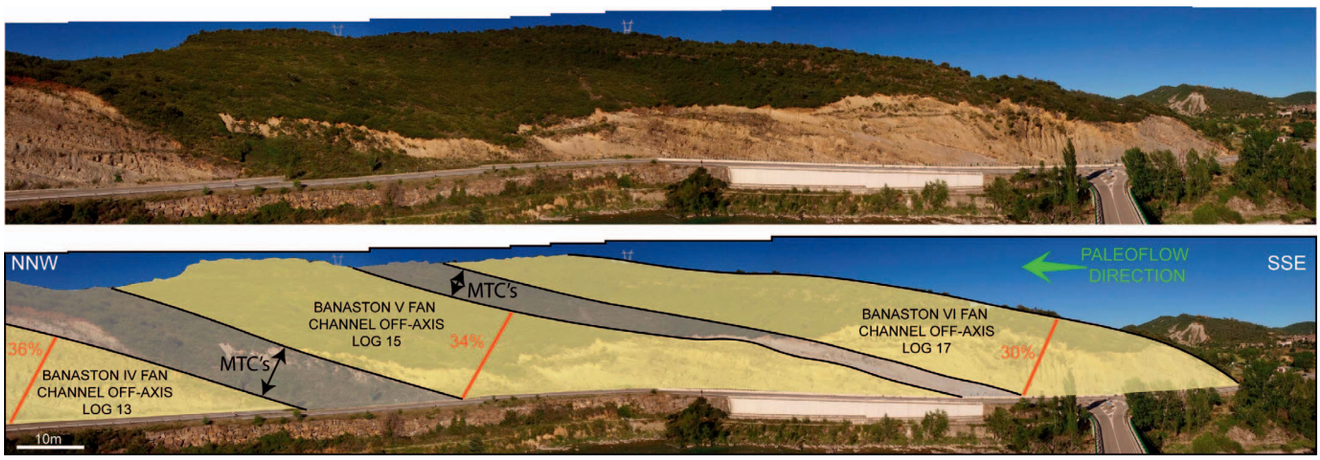

FIG. 8.—Panorama showing the channel off-axis of Banastón IV Fan (proximal basin-floor environments), the channel off-axis of Banastón V Fan (proximal basin-floor environments) and channel off-axis environments in the Banastón VI Fan, road section along N260, north of Boltaña. Percentages refer to the proportion of sediment interpreted as SFDs.

systems: the overall Fr still being supercritical, but generally lower than in the other Banastón fans.

Ainsa System (Lower-Slope Environment)

Interpretations of depositional environments of the Ainsa System and constituent fans are based on Pickering and Corregidor (2005) and Pickering et al. (2015).

Ainsa I Fan.—The closely spaced detailed sedimentary logs made in channel 1 of the Ainsa I Fan (< 400 m) militated against the clear recognition of any subtly different channel environment. Both logs (Table 1, Logs 19 and 20; Fig. 9) were measured in channel-axis environments in the Ainsa I Fan, and show a range in SFD distribution between 52 and 59%. However, the increase of mudstone percentage from Log 19 (18%) to Log 20 (33%), is consistent with the latter being a slightly more off-axis channel environment, albeit still within the main channel(s). Furthermore, the observation of the different types of supercritical-flow bedforms might aid in the discrimination of depositional environments. Log 19 contains several structures that can be interpreted as candidate cyclic steps, whereas Log 20 is characterized by deposits showing typical partial Bouma sequences (T_{abc}) where only the T_b division is interpreted as deposited under supercritical-flow conditions.

The study of another channel (channel 2) in the Ainsa I Fan was undertaken, where three detailed sedimentary logs were measured. In this case the sedimentary log in the channel axis is spaced ~ 2 km from the channel off-axis and channel-margin logs, thereby providing a clear distinction between the channel-axis and off-axis sites. The channel axis contains several thick- to medium-bedded, erosionally based structures, interpreted as candidate cyclic steps, most of which are associated with Facies Class B of Pickering and Hiscott (2016). The channel-margin environment contains more structures interpreted as deposited under subcritical-flow conditions, such as dune and current-ripple deposits. The study of channel 2 shows a large decrease of SFD proportion from the channel-axis site (61%) to the channel off-axis site (44%) and the channel-margin site (31%) (Table 1, Logs 21, 22, and 23).

Ainsa III Fan.—Two sedimentary logs were measured in the Ainsa III Fan. Several bedforms in the channel axis can be interpreted as unstable-antidune deposits (FA2a and FA2b), associated with a greater proportion of Facies Class B deposits (Pickering and Hiscott 2016) in the channel axis. The predominant deposits are fine- and medium-grained sandstones, both in channel-axis and channel off-axis sites, even where channel off-axis deposits contain more coarse-grained sandstones and conglomerates than do channel-axis sites. The Ainsa III Fan shows the largest decrease in the proportion of SFDs from channel axis to channel off-axis in the Ainsa Basin, i.e., from 66% to 34% (Table 1, Logs 24 and 25; Fig. 9). From these observations and interpretations, the Ainsa III Fan appears to have been dominated by depositional processes under supercritical-flow conditions. With the presence of conglomeratic and coarse-grained sandstones in channel off-axis environments, they can be interpreted as the vestiges of bedload bypass processes through the channel axis to depositional sites basinwards in the more distal parts of channels and lobes (Jaca Basin).

DISCUSSION

Our description and analysis of the distribution of SFDs in ancient submarine-fan channels and related environments has contributed to an improved understanding of the likely flow dynamics and depositional processes in deep-marine siliciclastic systems. Erosional coarse-grained supercritical-flow bedforms (FA1a and FA1b) are observed mainly in channel-axis sites, in relatively high-gradient, and in confined, basin settings (Gerbe System and at the base of the Banastón I and Ainsa I) (Fig. 10). The location of these bedforms towards the base of the sandy fans suggests that they could have been precursors to the development of channels in the Banastón I and Ainsa I fans. At a significantly larger scale, similar processes of active cyclic steps eroding a submarine canyon have been observed in the Monterey channel (Fildani et al. 2006) and in Eel Canyon, California (Lamb et al. 2008). Depositional fine-grained supercritical-flow bedforms (FA2a, FA2b, FA3, and FA4) are more common in low-gradient slopes and relatively unconfined settings, such as the Banastón II, III, IV, V, and VI and in the Ainsa III fans (Fig. 10). These facies associations are also present in channel-axis and off-axis sites. Upper-plane beds are observed from the channel-axis sites to the channel–levee–overbank sites. We acknowledge that a flow can be thicker than seabed topography, in which case a relatively unconfined flow could leave a confined deposit (e.g., in a large scour or large-aspect-ratio channel). We, therefore, use the terms "confined" and "unconfined" to indicate relative confinement based on mapping criteria.

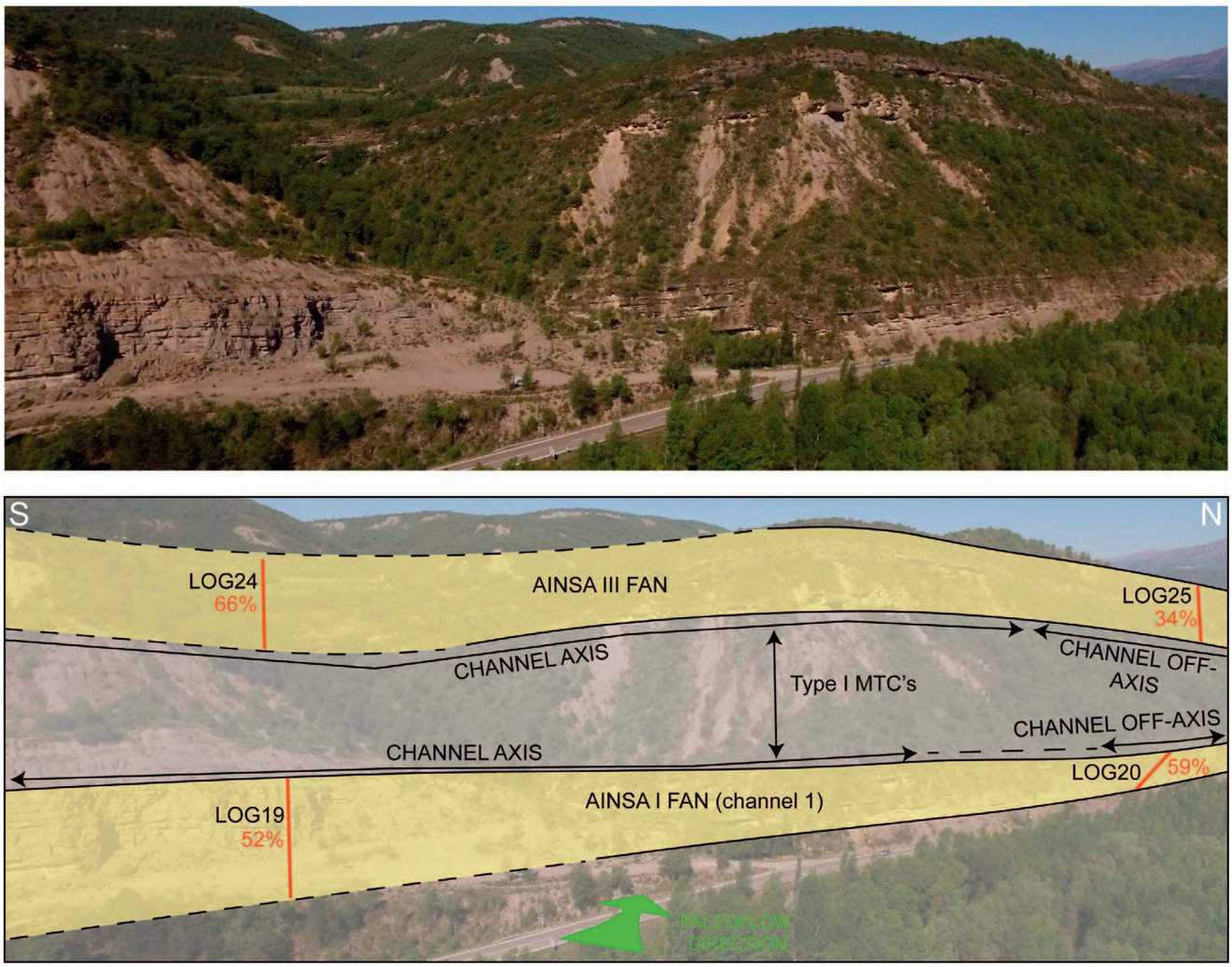

FIG. 9.—Panorama of the Ainsa I Fan (channel 1) and the Ainsa III Fan, separated by ~ 50 m of Type I MTCs (for definition, see Pickering and Corregidor 2005). The Ainsa I channel axis is interpreted to contain ~ 52% of SFDs, with 59% SFDs at the transition channel axis to off-axis. In contrast, the Ainsa III Fan channel axis has > 66% of SFDs, of which only 34% are SFDs in the channel off-axis sites.

SFD Distribution from Channel-Axis to Channel-Margin Sites

In the three studied systems in the Ainsa Basin (Gerbe, Banastón, and Ainsa), for most of the fans there is a decrease in the proportion of SFDs from channel-axis to channel-margin sites (Fig. 11). From channel-axis to channel-margin and levee–overbank sites, there is a systematic decrease in sandstone bed thickness and an increase in mudstone proportion, suggesting a lateral (axial-to-lateral) decrease in the strength of SGFs away from the channel axis. Similar SFD distributions and comparable interpretations were made by Lang et al. (2017a) for the upper Eocene Brito Formation (Nicaragua Basin), i.e., with an inferred decrease in flow strength (decrease in flow density and velocity) away from channel axes. Several researchers (e.g., Normark et al. 1980; Migeon et al. 2001; Fildani et al. 2006) observed supercritical-flow bedforms along channel margins or channel levees constructed by turbidity currents overspilling the confines of channels and creating crevasse splays or sediment slides. Very few candidate crevasse-splay structures were observed in the channel levee–overbank systems in the Ainsa Basin, which could explain why very few supercritical-flow bedforms were observed in channel-margin or levee–overbank environments.

SFD Distribution from Proximal to Distal Sites

When the percentage of SFDs is binned into different depositional environments, the data reveal an overall increase in the proportion of SFDs from the Gerbe (mid-lower slope), to Banastón (proximal-basin floor), and Ainsa (lower slope) systems (Fig. 11). Comparison between systems is linked with the SFD percentage in channel-axis sites where most of supercritical-flow bedforms are observed.

In the Gerbe System, a low percentage of SFDs is observed with 35% and 38% in the Gerbe I and Gerbe II fans, respectively (Fig. 11). Because these are mid-lower slope environments, with likely slope gradients >> 0.5°, a higher percentage of SFDs was expected. Concentrated density flows and turbidity currents can have substantial erosional potential to create scour structures at least partially infilled with conglomerate and coarse-grained sandstones that otherwise might have bypassed these sites (cf. Wynn et al. 2002; Macdonald et al. 2011; Ito et al. 2014). In such cases, one would not expect the formation of supercritical-flow bedforms in the conglomerate-dominated Gerbe I Fan, i.e., resulting in the observed low percentage of SFDs. Furthermore, lens-shaped conglomeratic layers, pebbly sandstones, and truncated sandstone beds are a common feature in the Gerbe System,

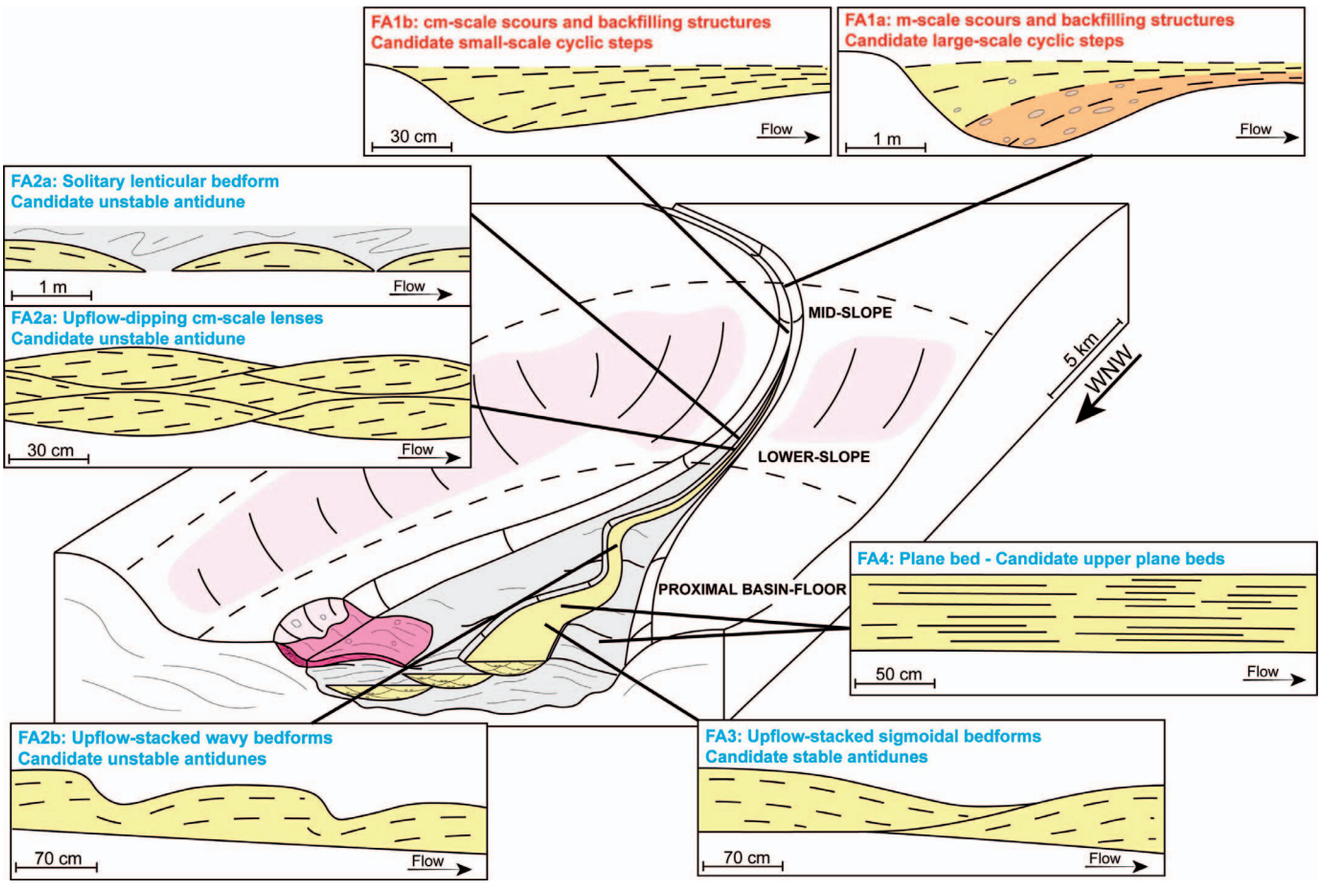

FIG. 10.—Schematic depositional model for the Ainsa Basin sandy fans to show the environmental distribution of the six facies associations with SFDs. The SFDs occur across a wide range of environments but are shown where they are most abundant. Erosional coarse-grained supercritical-flow bedforms (red) are dominant in channel-axis environments in relatively confined settings, and also high slope gradients such as in the mid-slope and transition between middle- to lower-slope environments. Depositional fine-grained supercritical-flow bedforms (blue) are the dominant facies association in channel-axis and off-axis sites in relatively unconfined settings, and in relatively low-gradient slope sites.

and can be considered as characteristic of sediment bypass. The increased proportion of SFDs in the Gerbe II Fan (compared with that in the Gerbe I Fan) can be explained by decreased confinement of the fan, all consistent with mapping (Pickering and Bayliss 2009). A decrease in confinement will lead to a flow that spreads more laterally, therefore the flow will be thinner. The Fr is directly linked with the flow height. For the same sediment concentration and flow discharge, if the flow height decreases, the Fr increases in the density flow; thereby, the flow is more likely to produce supercritical bedforms. There is also an increase in the proportion of fine-grained sediment (medium- to fine-grained sandstones) from the Gerbe I to the Gerbe II Fan, an observation that we believe is coincidental rather than resulting from any genetic association, i.e., this represents local preservation from a time when there was more sediment bypass in the Gerbe I compared with the Gerbe II Fan. The Gerbe System was deposited during the terminal stage of a period of intense tectonic shortening and deformation associated with folding, thrusting, and local overturning of the underlying Arro System (Millington and Clark 1995; Pickering and Cantalejo 2015). The generally low percentage of SFDs in the Gerbe System can be explained by deposition during the development of a new system of canyon and submarine channel following basin reorganization, with sandy SGFs generally having been strongly erosional rather than depositional, thereby generating more erosional structures rather than supercritical-flow depositional structures. Mapping by Pickering and Bayliss (2009) has suggested that, unlike in many continental margins, sandy fans in the Ainsa Basin were separated by tens to hundreds of meters of basin-wide fine-grained sediment accumulation that infilled and healed any point sources that provided coarse siliciclastics to older fans.

In the Banastón System, the transition from middle to lower slope to proximal basin-floor environments resulted in an overall decrease of confinement (Pickering and Bayliss 2009; Bayliss and Pickering 2015). During deposition of the Banastón I, II, and III fans (compared with the later Banastón IV, V, and VI fans), the growth of the Añisclo Anticline likely ceased or the sediment accumulation rate exceeded the growth of the Añisclo Anticline, resulting in a progressive decrease in lateral confinement. The Banastón I Fan has the highest proportion of coarse-grained sediment (including conglomerates) in the Banastón System, and with one of the lowest proportions of SFDs (37%). In contrast, the Banastón II Fan shows a greater percentage of SFDs (58%) which can be linked to decreased confinement compared with that for the Banastón I Fan. The decrease in the proportion of conglomerates and coarse-grained sandstones from the Banastón I to the Banastón II Fan can be explained by more sediment bypass in the Banastón I Fan, with a lower preservation of SFDs in the latter. The Banastón III Fan has ~ 45% SFDs, a value significantly lower than the underlying Banastón II Fan but greater than the Banastón I Fan. Whilst mapping of the Banastón III Fan shows that it is the least confined sandy fan of the Banastón I, II, and III fans, it has the

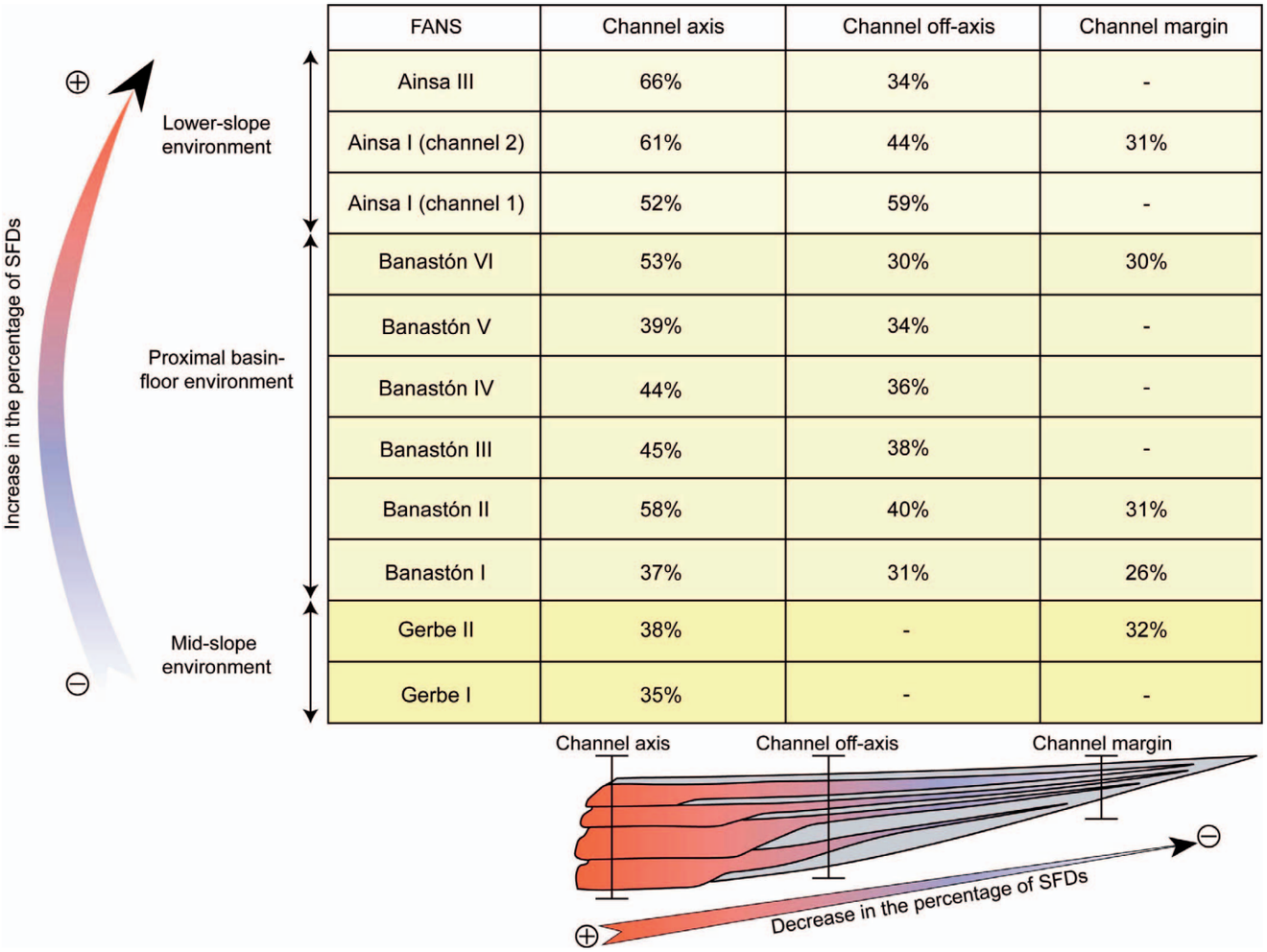

FANS	Channel axis	Channel off-axis	Channel margin
Ainsa III	66%	34%	-
Ainsa I (channel 2)	61%	44%	31%
Ainsa I (channel 1)	52%	59%	-
Banastón VI	53%	30%	30%
Banastón V	39%	34%	-
Banastón IV	44%	36%	-
Banastón III	45%	38%	-
Banastón II	58%	40%	31%
Banastón I	37%	31%	26%
Gerbe II	38%	-	32%
Gerbe I	35%	-	-

FIG. 11.—Variation in proportion of SFDs in an axial-to-lateral direction. Note the decrease in the proportion of SFDs from channel-axis to channel-margin sites, and between the different systems, with an increase in SFDs from the Gerbe System (mid-slope environments), to the Banastón System (proximal basin-floor environments), and to the Ainsa System (lower-slope environments). This increase is seen in the channel-axis environments of each system, where most of the supercritical-flow bedforms were recorded.

thickest MTDs (up to ~ 20 m), as well as abundant MTDs and, therefore, is likely to have been associated with substantial lateral confinement of sands due to reduced accommodation space created by depositional topography. Thus, in any discussion of the proportion of SFDs, it is important to distinguish between both system-wide confinement (between the basin-bounding growth anticlines) and more local confinement caused by the deposition of MTDs.

In the Banastón IV, V, and VI fans, there is no change in the thickness of sandbodies across the Añisclo Anticline, interpreted as due to essentially no growth of this seafloor high during sandy-fan deposition (Bayliss and Pickering 2015). This lack of significant syndepositional tectonic activity resulted in a progressive decrease of confinement from the Banastón IV to Banastón VI fans. The decreased lateral confinement of these fans resulted in a progressive increase in the proportion of SFDs from the Banastón IV Fan (44%) to the Banastón VI Fan (53%) (Fig. 11). Symons et al. (2016) and Covault et al. (2016) show that large-scale fine-grained sediment waves are most likely to develop in unconfined settings.

In the Ainsa System, the high proportion of SFDs is attributed to it being a lower-slope environment (in the SE of the Ainsa Basin, where the data for this study was collected) with relatively steep gradients compared with the Banastón System. The Ainsa System also has a higher percentage of fine- to medium-grained sandstones compared with the Gerbe System, suggesting less sediment bypass than in the Gerbe System. Additionally, the Ainsa System shows a transition from lower-slope to proximal basin-floor environments (Pickering and Corregidor 2005; Pickering et al. 2015). In such a setting, transiting SGFs are very likely to have experienced hydraulic jumps at the break of slope associated with a rapid decrease of lateral confinement, all conductive to the generation of supercritical-flow bedforms.

The Ainsa I Fan shows greater lateral confinement compared with the Ainsa II and III fans, most likely due to the presence of both underlying and laterally deposited Type I MTCs, which created substantial irregular topography and locally ponded accommodation (Pickering et al. 2015). Fan lateral confinement can explain the relatively low percentage of SFD of the Ainsa I Fan compared to Ainsa II and III fans (Fig. 11). Throughout deposition of the Ainsa System, relatively little significant intrabasinal tectonic activity favored a progressive decrease in lateral confinement from the Ainsa I to Ainsa III fans. The Ainsa III Fan contains the highest proportion of fine-grained sediments and, based on mapping (Pickering et al. 2015), was the least confined fan, showing the highest proportion of SFDs, with 66% of the total channel-axis deposits (Fig. 11).

Parameters Influencing SGF Criticality

In this study, two main parameters are recognized as having played an important role on the hydrodynamics of SGFs (i.e., if the flow was under supercritical or subcritical conditions): (i) lateral confinement of the sandy fans, and (ii) seafloor gradient. In the Ainsa Basin, these parameters vary both within and between depositional environments. At present, it is difficult to assess which of these parameters (above) might have exerted the greatest influence in determining the criticality of any SGF. However, in ancient systems such as in the Ainsa Basin, mapping makes confinement easier to recognize than subtle differences in seafloor gradient.

Concerning confinement, a greater proportion of fine-grained SFDs were observed in relatively unconfined (compared with more confined) settings. However, this observation does not preclude SGFs being under supercritical-flow conditions in confined settings. Most of the SFDs observed in relatively confined settings are coarse-grained erosional bedforms with a strong erosional component, and bedforms likely formed under the highest Fr. In relatively unconfined settings, fine-grained depositional supercritical-flow bedforms are the dominant SFDs and form at lower Fr (but $Fr > 1$). We suspect that the preservation potential of SFDs is greatest in relatively unconfined systems, due to deceleration of SGFs at the transition from a relatively confined system (mid-slope environment—Gerbe System) to a relatively unconfined system (break-of-slope, lower-slope, and proximal basin-floor environments—Banastón and Ainsa systems). We suspect that there is a trade-off between confinement of sandbodies and slope gradient, with both playing a role in the criticality of a flow and in the preservation of any supercritical-flow bedforms, e.g., we observe the highest percentage of SFDs in the Ainsa System (lower-slope environment) which shows moderate confinement and intermediate slope gradient.

SFDs or Tidal Deposits?

A curious aspect of the Ainsa Basin is that many of the deposits we describe and interpret here appear to be poorly documented from other ancient deep-marine systems. This might simply be that such bedforms have been overlooked in the past, because they have not fitted expected depositional models, including the Bouma sequence. Alternatively, one might argue that they could represent a deep-water tidal influence in the Ainsa Basin, which was certainly a narrow and elongate seaway connected to the global ocean, perhaps with similarities to submarine canyons, where tidal processes are recognized in deep water (e.g., Beaulieu and Baldwin 1998). The absence of candidate tidal bundling (e.g., neap–spring depositional cycles), a lack of convincing flaser, wavy, and lenticular ripples, and the ubiquitous presence of deep-water foraminifera, leads us to reject this interpretation in favor of processes linked to supercritical versus subcritical flow in SGFs.

CONCLUSIONS

In this paper, we describe a large range of sedimentary structures, bedforms, and deposits from the middle Eocene deep-marine Ainsa Basin that were likely deposited under supercritical-flow conditions. From field observations, we propose six facies associations related to supercritical SGFs. These facies associations are binned in two categories:

(i) Erosional coarse-grained supercritical-flow bedforms, commonly observed in relatively confined settings such as mid- to lower-slope environments. These bedforms are associated with meter and centimeter scale scour-and-backfilling structures, interpreted as candidate large-scale cyclic steps and small-scale cyclic steps.

(ii) Depositional fine-grained supercritical-flow bedforms, commonly observed in intrachannel sites in relatively unconfined settings, such as base-of-slope, break-of-slope, and proximal basin-floor environments. These bedforms are related to upflow-dipping sandstone lenses, upflow-stacked wavy bedforms, upflow-stacked sigmoidal bedforms, and plane beds interpreted as unstable and stable antidunes and UFR plane beds.

We demonstrate the importance of determining the relative proportion of SFDs in different submarine-fan and related environments as a tool for improving the understanding of likely flow dynamics in deep-water siliciclastic systems. We have produced an erosional–depositional model for this distribution of structures, bedforms, and deposits, something that should prove useful for comparison with other deep-water systems. In this study, we have determined the distribution of supercritical-flow bedforms in the Ainsa Basin, showing that it varies with:

(i) Axial-lateral changes: a decrease in the proportion of SFDs from channel-axis to the channel-margin environments, interpreted as due to decreased flow strength from channel axis to channel margin.

(ii) Proximal-to-distal changes: an increase in the proportion of SFDs from the older Gerbe (mid-lower-slope, coarsest-grained fans), to Banastón System (proximal-basin-floor environment), and to the younger Ainsa System (lower-slope environments with the relatively finest-grained fans of all three systems).

The parameters that appear to have the most impact on the criticality of a flow are the relative confinement and seafloor gradient, and not grain size. We would argue that any apparent genetic association between the proportion of SFDs and grain size is coincidental and related to preservation potential. Tectonic activity, such as the growth of the Mediano, Boltaña, and Añisclo anticlines, will have played an important role in the confinement of the fans (and also in slope gradient), thereby impacting the criticality of any flows.

Until further studies similar to ours are conducted in other ancient deep-water depositional systems, we do not know how typical our values for SFDs (channel axis, from 35% to 66%; channel off-axis, from 30% to 59%; channel margin, from 26% to 30%) might be to characterize channel and related environments. This study is a first step in the recognition and evaluation of SFDs in deep-marine environments. More work is required to understand the mechanics of sediment gravity flows. From this paper, several questions arise, such as: how common are these SFDs in others deep-water systems with basin settings different from that of the Ainsa Basin (basin width and length, slope gradient, or water depth). How do we evaluate the difference in scale between structures observed in ancient and modern deep-water systems but also structures obtained in flume-tank experiments? What are the typical values for Fr, flow density, ambient fluid, flow depth? Based on field observations only, these questions are difficult to answer. There is, therefore, a need to be combine field observations and measurements with results from flume experiments and numerical modeling, and with observation of sediment gravity flows and their deposits in modern systems.

ACKNOWLEDGEMENTS

We thank Hess Corporation (in particular Richard Beaubouef and Scott Pluim) and University College London (UCL) for funding this research. We thank Rick Hiscott (Memorial University, Newfoundland) for his constructive criticism, which has led to a much-improved paper. We would also like to thank Matthieu Cartigny, Andrea Fildani, Bill Arnott, Marco Patacci, and John Southard for their helpful comments.

REFERENCES

Alexander, J., and Fielding, C., 1997, Gravel antidunes in the tropical Burdekin River, Queensland, Australia: Sedimentology, v. 44, p. 327–337.

Alexander, J., Bridge, J.S., Cheel, R.J., and Leclair, S.F., 2001, Bedforms and associated sedimentary structures formed under supercritical water flows over aggrading sand beds: Sedimentology, v. 48, p. 133–152.

Allen, J.R.L., 1982, Sedimentary Structures; Their Character and Physical Basis, Volume 1: New York, Elsevier, 593 p.

Allen, J.R.L., 1984, Parallel lamination developed from upper-stage plane beds: a model based on the larger coherent structures of the turbulent boundary layer: Sedimentary Geology, v. 39, p. 227–242.

Arnott, R.W.C., and Al-Mufti, O., 2017, Deep-marine pseudo dune cross-stratification: similar, but completely different: Journal of Sedimentary Research, v. 87, p. 312–323. doi:10.2110/jsr.2017.21

Bayliss, N.J., and Pickering, K.T., 2015, Transition from deep-marine lower-slope erosional channels to proximal basin-floor stacked channel–levée–overbank deposits, and syn-sedimentary growth structures, Middle Eocene Banastón System, Ainsa Basin, Spanish Pyrenees: Earth-Science Reviews, v. 144, p. 23–46.

Beaulieu, S., and Baldwin, R., 1998, Temporal variability in currents and the benthic boundary layer at an abyssal station off central California: Deep-Sea Research, Part II, v. 45, p. 587–615.

Carling, P.A., and Schvidchenko, A.B., 2002, A consideration of the dune: antidune transition in fine gravel: Sedimentology, v. 49, p. 1269–1282.

Cartigny, M.J.B., Postma, G., Van Den Berg, J.H., and Mastbergen, D.R., 2011, A comparative study of sediment waves and cyclic steps based on geometries, internal structures and numerical modelling: Marine Geology, v. 280, p. 40–56.

Cartigny, M.J.B., Ventra, D., Postma, G., and Can Den Berg, J.H., 2014, Morphodynamics and sedimentary structures of bedforms under supercritical-flow conditions: new insights from flume experiments: Sedimentology, v. 61, p. 712–748.

Cheel, R.J., 1990, Horizontal lamination and the sequence of bed phase and stratification under upper-flow-regime conditions: Sedimentology, v. 37, p. 517–529.

Clark, J.D., and Pickering, K.T., 1996, Architectural elements and growth patterns of submarine channels: application to hydrocarbon exploration: American Association of Petroleum Geologists, Bulletin, v. 80, p. 194–221.

Covault, J.A., Kostic, S., Paull, C.K., Ryan, H.F., and Fildani, A., 2014, Submarine channel initiation, filling and maintenance from sea-floor geomorphology and morphodynamic modelling of cyclic steps: Sedimentology, v. 61, p. 1031–1054.

Covault, J.A., Kostic, S., Paull, C.K., Sylverster, Z., and Fildani, A., 2016, Cyclic steps and related supercritical bedforms: building blocks of deepwater depositional systems, western North America: Marine Geology, v. 393, p. 4–20.

Dorrell, R.M., Peakall, J., Sumner, E.J., Parsons, D.R., Darby, S.E., Wynn, R.B., Özsoy, E., and Tezcan, D., 2016, Flow dynamics and mixing processes in hydraulic jump arrays: implications for channel–lobe transition zones: Marine Geology, v. 381, p. 181–193.

Fedele, J.J., Hoyal, D., Barnaal, Z., Tullenko, J., and Awalt, S., 2016, Bedforms created by gravity currents, *in* Budd, D.A., Hajek, E.A., and Purkis, S.J., eds., Autogenic Dynamics and Self-Organization in Sedimentary Systems: SEPM, Special Publication 106, p. 95–121.

Fielding, C.R., 2006, Upper flow regime sheets, lenses and scour fills: extending the range of architectural elements for fluvial sediment bodies: Sedimentary Geology, v. 190, p. 227–240.

Fildani, A., Normark, W.R., Kostic, S., and Parker, G., 2006, Channel formation by flow stripping: large-scour features along the Monterey East Channel and their relation to sediment waves: Sedimentology, v. 53, p. 1265–1287.

Garcia, M.H., 1993, Hydraulic jumps in sediment-driven bottom currents: Journal of Hydraulic Engineering, v. 119, p. 1094–1117.

Garcia, M., and Parker, G., 1989, Experiments on hydraulic jumps in turbidity currents near a canyon–fan transition: Science, v. 245, p. 393–396.

Gilbert, G.K., 1914, The transportation of debris by running water: U.S. Geological Survey, Professional Paper 86, p. 15–263.

Guy, H.P., Simons, D.B., and Richardson, E.V., 1966, Summary of alluvial channel data from flume experiments 1956–1961: U.S. Geological Survey, Professional Paper 461, p. 11–96.

Hage, S., Cartigny, M.J.B., Clare, M.A., Sumner, E.J., Vendettuoli, D., Hughes Clarke, J.E., Hubbard, S.M., Talling, P.J., Lintern, D.G., Stacey, C.D., Englert, R.G., Vardy, M.E., Hunt, J.E., Yokokawa, M., Parsons, D.R., Hizzett, J.L., Azpiroz-zabala, M., and Vellinga, A.J., 2018, How to recognize crescentic bedforms formed by supercritical turbidity currents in the geologic record: insights from active submarine channels: Geology, v. 46, p. 563–566.

Hand, B.M., Middleton, G.V., and Skipper, K., 1972, Antidune cross-stratification in a turbidite sequence, Cloridorme Formation, Gaspé, Québec: Sedimentology, v. 18, p. 135–138.

Hand, B.M., 1974, Supercritical flow in density currents: Journal of Sedimentary Petrology, v. 44, p. 637–648.

Hiscott, R.N., 1994, Traction-carpet stratification in turbidites: fact or fiction?: Journal of Sedimentary Research, v. 64, p. 204–208.

Hiscott, R.N., and Middleton, G.V., 1979, Depositional mechanics of thick-bedded sandstones at the base of a submarine slope, Tourelle Formation (Lower Ordovician), Québec, Canada, *in* Doyle, L.J., and Pilkey, O.H., eds., Geology of Continental Slopes: Society of Economic Paleontologists and Mineralogists, Special Publication 27, p. 307–326.

Hofstra, M., Hodgson, D.M., Peakall, J., and Flint, S., 2015, Giant scour-fills in ancient channel–lobe transition zones: formative processes and depositional architecture: Sedimentary Geology, v. 329, p. 98–114.

Hughes Clarke, J.E., 2016, First wide-angle view of channelized turbidity currents links migrating cyclic steps to flow characteristics: Nature Communications, v. 7, no. 11896.

Hughes Clarke, J.E., Brucker, S., Muggah, J., Church, I., and Cartwright, D., 2011, The Squamish delta repetitive survey program: a simultaneous investigation of prodeltaic sedimentation and integrated system accuracy: Squamish Repetitive Survey Program, Mapping-5, U.S. Hydrographic Conference 2011, 16 p.

Hughes Clarke, J.E., Brucker, S., Muggah, J., Church, I., Cartwright, D., Kuus, P., Hamilton, T., Pratamo, D., and Eisan, B., 2012, The Squamish prodelta: monitoring active landslides and turbidity currents: The Arctic, Old Challenges New, Niagara Falls, Canada.

Ito, M., Ishikawa, K., and Nishida, N., 2014, Distinctive erosional and depositional structures formed at a canyon mouth: a lower Pleistocene deep-water succession in the Kazusa forearc basin on the Boso Peninsula, Japan: Sedimentology, v. 61, p. 2042–2062.

Jopling, A.V., and Richardson, E.V., 1966, Backset bedding developed in shooting flow in laboratory experiments: Journal of Sedimentary Petrology, v. 36, p. 821–825.

Kennedy, J.F., 1961, Stationary Waves and Antidunes in Alluvial Channels: California Institute of Technology, W.M. Keck Laboratory of Hydraulics and Water Research, Report KH R-2, 146 p.

Komar, P.D., 1971, Hydraulic jumps in turbidity currents: Geological Society of America, Bulletin, v. 82, p. 1477–1487.

Kostic, S., and Parker, G., 2006, The response of turbidity currents to a canyon–fan transition: internal hydraulic jumps and depositional signatures: Journal of Hydro-environmental Research, v. 44, p. 631–653.

Kostic, S., Sequeiros, O., Spinewine, B., and Parker, G., 2010, Cyclic steps: a phenomenon of supercritical shallow flow from the high mountains to the bottom of the ocean: Journal of Hydro-environmental Research, v. 3, p. 167–172.

Lamb, M.P., Parsons, J.D., Mullenbach, B.L., Finlayson, D.P., Orange, D.L., and Nittrouer, C.A., 2008, Evidence for superelevation, channel incision, and formation of cyclic steps by turbidity currents in Eel Canyon, California: Geological Society of America, Bulletin, v. 120, p. 463–475.

Lang, J., and Winsemann, J., 2013, Lateral and vertical facies relationship of bedforms deposited by aggrading supercritical flow: from cyclic steps to humpback dunes: Sedimentary Geology, v. 296, p. 36–54.

Lang, J., Brandes, C., and Winsemann, J., 2017a, Erosion and deposition by supercritical density flows during channel avulsion and backfilling: field examples from coarse-grained deep-water channel–levée complexes (Sandino Forearc Basin, southern Central America): Sedimentary Geology, v. 349, p. 79–102.

Lang, J., Sievers, J., Loewer, M., Igel, J., and Winsemann, J., 2017b, 3D architecture of cyclic-step and antidune deposits in glaciogenic subaqueous fan and delta settings: integrating outcrop and ground-penetrating radar data: Sedimentary Geology, v. 362, p. 83–100.

Langford, R., and Bracken, B., 1987, Medano Creek, Colorado, a model for upper-flow-regime fluvial deposition: Journal of Sedimentary Petrology, v. 55, p. 863–870.

Lennon, J.M., and Hill, D.F., 2006, Particle image velocimetry measurements of undular and hydraulic jumps: Journal of Hydraulic Engineering, v. 132, p. 1283–1294.

Macdonald, R.G., Alexander, J., Bacon, J.C., and Cooker, M.J., 2009, Flow patterns, sedimentation and deposit architecture under a hydraulic jump on a non-eroding bed: defining hydraulic-jump unit bars: Sedimentology, v. 56, p. 1346–1367.

Macdonald, H.A., Wynn, R.B., Huvenne, V.A.I., Peakall, J., Masson, D.G., Weaver, P.P.E., and Mcphail, S.D., 2011, New insights into the morphology, fill, and remarkable longevity (> 0.2 m.y.) of modern deep-water erosional scours along the northeast Atlantic margin: Geosphere, v. 7, p. 845–867.

Massari, F., 1996, Upper-flow-regime stratification types on steep-faced, coarse-grained, Gilbert-type progradational wedges (Pleistocene, southern Italy): Journal of Sedimentary Research, v. 66, p. 364–375.

Massari, F., 2017, Supercritical-flow structures (backset-bedded sets and sediment waves) on high-gradient clinoform systems influenced by shallow-marine hydrodynamics: Sedimentary Geology, v. 360, p. 73–95.

Massari, F., and Parea, G.C., 1990, Wave-dominated Gilbert-type gravel deltas in the hinterland of the Gulf of Taranto (Pleistocene, southern Italy), *in* Colella, A., and Prior, D.B., eds., Coarse-grained Deltas: International Association of Sedimentologists, Special Publication 10, p. 311–331.

Middleton, G.V., 1965, Antidune cross-bedding in a large flume: Journal of Sedimentary Petrology, v. 35, p. 922–927.

Migeon, S., Savoye, B., Zanella, E., Mulder, T., Faugères, J.C., and Weber, O., 2001, Detailed seismic-reflection and sedimentary study of turbidite sediment waves on the Var Sedimentary Ridge (SE France): significance for sediment transport and deposition and for the mechanisms of sediment-wave construction: Marine and Petroleum Geology, v. 18, p. 179–208.

Millington, J.J., and Clark, J.D., 1995, The Charo–Arro canyon-mouth sheet system, south-central Pyrenees, Spain: a structurally influenced zone of sediment dispersal: Journal of Sedimentary Research, v. 65, p. 443–454.

Mulder, T., Razin, P., and Faugères, J.C., 2009, Hummocky cross-stratification-like structures in deep-sea turbidites: upper Cretaceous Basque basins (Western Pyrenees, France): Sedimentology, v. 56, p. 997–1015.

Muñoz, J.A., 1992, Evolution of a continental collision belt: ECORS–Pyrenean crustal balanced section, *in* McClay, K.R., ed., Thrust Tectonics: New York, Chapman and Hall, p. 235–246.

Muñoz, J.A., Beamud, E., Fernández, O., Arbués, P., Dinarès-Turell, J., and Poblet, J., 2013, The Ainsa fold and thrust oblique zone of the central Pyrenees: kinematics of a curved contractional system from paleomagnetic and structural data: Tectonics, v. 32, p. 1142–1175.

Mutti, E., and Normark, W.R., 1987, Comparing examples of modern and ancient turbidite systems: problems and concepts, *in* Leggett, J.K., and Zuffa, G.G., eds., Marine Clastic Sedimentology, Concepts and Case Studies: London, Graham and Trotman, p. 1–38.

Mutti, E., and Normark, W.R., 1991, An integrated approach to the study of turbidite systems, Seismic Facies and Sedimentary Processes of Submarine Fans and Turbidite Systems: New York, Springer, p. 75–106.

Normark, W.R., Hess, G.R., Stow, D.A.V., and Bowen, A.J., 1980, Sediment waves on the Monterey Fan levee: a preliminary physical interpretation: Marine Geology, v. 37, p. 1–18.

Normandeau, A., Lajeunesse, P., Poire, A.G., and Francus, P., 2016, Morphological expression of bedforms formed by supercritical sediment density flows in four fjord-lake deltas of the south-eastern Canadian Shield (Eastern Canada): Sedimentology, v. 63, p. 2106–2129.

Ono, K., and Plink-Björklund, P., 2017, Froude supercritical flow bedforms in deepwater slope channels? Field examples in conglomerates, sandstones and fine-grained deposits: Sedimentology, v. 65, p. 639–669.

Paola, C., Wiele, S.M., and Reinhart, M.A., 1989, Upper-regime parallel lamination as the result of turbulent sediment transport and low-amplitude bedforms: Sedimentology, v. 36, p. 47–59.

Paull, C.K., Ussler, W., III, Caress, D.W., Lundsten, E., Covault, J.A., Maier, K.L., Xu, J., and Augenstein, S., 2010, Origins of large crescent-shaped bedforms within the axial channel of Monterey Canyon, offshore California: Geosphere, v. 6, p. 755–774.

Pickering, K.T., and Bayliss, N.J., 2009, Deconvolving tectono-climatic signals in deep-marine siliciclastics, Eocene Ainsa Basin, Spanish Pyrenees: seesaw tectonics versus eustasy: Geology, v. 37, p. 203–206.

Pickering, K.T., and Cantalejo, B., 2015, Deep-marine environments of the Middle Eocene Upper Hecho Group, Spanish Pyrenees: Introduction: Earth-Science Reviews, v. 144, p. 1–9.

Pickering, K.T., and Corregidor, J., 2005, Mass-transport complexes (MTCs) and tectonic control on basin-floor submarine fans, middle Eocene, South Spanish Pyrenees: Journal of Sedimentary Research, v. 75, p. 761–783.

Pickering, K.T., and Hiscott, R.N., 1985, Contained (reflected) turbidity currents from the Middle Ordovician Cloridorme Formation, Quebec, Canada: an alternative to the antidune hypothesis: Sedimentology, v. 32, p. 373–394.

Pickering, K.T., and Hiscott, R.N., (with contribution from T. Heard), 2016, Deep Marine Systems: Processes, Deposits, Environments, Tectonic and Sedimentation: Wiley/American Geophysical Union, 672 p.

Pickering, K.T., Stow, D.A.V., Watson, M.P., and Hiscott, R.N., 1986, Deep-water facies, processes and models: a review and classification scheme for modern and ancient sediments: Earth-Science Reviews, v. 23, p. 75–174.

Pickering, K.T., Corregidor, J., and Clark, J.D., 2015, Architecture and stacking patterns of lower-slope and proximal basin-floor channelized submarine fans, Middle Eocene Ainsa System, Spanish Pyrenees: an integrated outcrop: subsurface study: Earth-Science Reviews, v. 144, p. 82–106.

Piper, D.J., and Normark, W.R., 2001, Sandy fans: from Amazon to Hueneme and beyond: American Association of Petroleum Geologists, Bulletin, v. 85, p. 1407–1438.

Postma, G., and Cartigny, M.J.B., 2014, Supercritical and subcritical turbidity currents and their deposits: a synthesis: Geology, v. 42, p. 987–990.

Postma, G., Cartigny, M.J.B., and Kleverlaan, K., 2009, Structureless, coarse-tail graded Bouma T_a formed by internal hydraulic jump of the turbidity current?: Sedimentary Geology, v. 219, p. 1–6.

Postma, G., Kleverlaan, K., and Cartigny, M.J.B., 2014, Recognition of cyclic steps in sandy and gravelly turbidite sequences, and consequences for the Bouma facies model: Sedimentology, v. 61, p. 2268–2290.

Postma, G., Hoyal, D.C., Abreu, V., Cartigny, M.J.B., Demko, T., Fedele, J.J., Kleverlaan, K., and Pederson, K.H., 2016, Morphodynamics of supercritical turbidity currents in the channel–lobe transition zone, *in* Lamarche, G., Mountjoy, J., Bull, S., Hubble, T., Krastel, S., Lane, E., Micallef, A., Moscardelli, L., Mueller, C., Pecher, I., and Woelz, S., eds., Submarine Mass Movements and Their Consequences: Advances in natural and Technological Hazards Research: Springer, v. 41, p. 469–478.

Remacha, E., Oms, O., Gual, G., Bolano, F., Climent, F., Fernández, L.P., Crumeyrollle, P., Pettingill, H., Vicente, J.C., and Suarez, J., 2003, Sand-rich turbidite systems of the Hecho Group from slope to basin plain facies, stacking patterns, controlling factors and diagnostic features: American Association of Petroleum Geologists, International Conference and Exhibition, Barcelona, Spain, Geological Field Trip 12.

Russell, H.A.J., and Arnott R.W.C., 2003, Hydraulic-jump and hyperconcentrated-flow deposits of a glacigenic subaqueous fan: Oak Ridges moraine, southern Ontario, Canada: Journal of Sedimentary Research, v. 73, p. 887–905.

Simons, D.B., Richardson, E.V., and Nordin, C.F., 1965, Sedimentary structures generated by flow in an alluvial channel, *in* Primary Sedimentary Structures and their Hydrodynamic Interpretation, Middleton, G.V.: SEPM, Special Publications 12, p. 34–52.

Skipper, K., 1971, Antidune cross-stratification in a turbidite sequence, Cloridorme Formation, Gaspé, Quebec: Sedimentology, v. 17, p. 51–68.

Slootman, A., Cartigny, M.J.B., Moscariello, A., Chiaradia, M., and De Boer, P.L., 2016, Quantification of tsunami-induced flows on a Mediterranean carbonate ramp reveals catastrophic evolution: Earth and Planetary Science Letters, v. 444, p. 192–204.

Spinewine, B., Sequeiros, O.E., Garcia, M.H., Beaubouef, R.T., Sun, T., and Savoye, B., 2009, Experiments on wedge-shaped deep-sea sedimentary deposits in mini basins and/or on channel–levees emplaced by turbidity currents. Part II. Morphodynamic evolution of the wedge and of the associated bedforms: Journal of Sedimentary Research, v. 79, p. 608–628.

Sumner, E.J., Peakall, J., Parsons, D., Wynn, R., Darby, S., Dorrell, R., Mcphail, S., Perett, J., Webb, A., and White, D., 2013, First direct measurements of hydraulic jumps in an active submarine density current: Geophysical Research Letters, v. 40, p. 5904–5908.

Symons, W.O., Sumner, E.J., Talling, P.J., Cartigny, M.J.B., and Clare, M.A., 2016, Large-scale sediment waves and scours on the modern seafloor and their implications for the prevalence of supercritical flows: Marine Geology, v. 371, p. 130–148.

Taki, K., and Parker, G., 2005, Transportational cyclic steps created by flow over an erodible bed. Part 1. Experiments: Journal of Hydraulic Research, v. 43, p. 488–501.

Tilston, M., Arnott, R.W.C., Rennie, C.D., and Long, B., 2015, The influence of grain size on the velocity and sediment concentration profiles and depositional record of turbidity currents: Geology, v. 43, p. 839–842.

Vellinga, A.J., Cartigny, M.J.B., Eggenhuisen, J.T., and Hansen, E.W.M., 2017, Morphodynamics and depositional signature of low-aggradation cyclic steps: new insights from a depth-resolved numerical model: Sedimentology, v. 65, p. 540–560.

Walker, R.G., 1965, The origin and significance of the internal sedimentary structures of turbidites: Yorkshire Geological Society, Proceedings, v. 35, p. 1–32.

Walker, R.G., 1967, Turbidite sedimentary structures and their relationship to proximal and distal depositional environments: Journal of Sedimentary Petrology, v. 37, p. 25–43.

Weirich, F.H., 1988, Field evidence for hydraulic jumps in subaqueous sediment gravity flows: Nature, v. 332, p. 626–629.

Winsemann, J., Brandes, C., and Polom, U., 2011, Response of a proglacial delta to rapid high amplitude lake-level change: an integration of outcrop data and high-resolution shear wave seismics: Basin Research, v. 23, p. 22–52.

Winterwerp, J.C., Bakker, W.T., Mastbergen, D.R., and Van Rossum, H., 1992, Hyperconcentrated sand–water mixture flows over erodible bed: Journal of Hydraulic Engineering, v. 118, p. 1508–1525.

Wynn, R.B., Piper, D.J., and Gee, M.J., 2002, Generation and migration of coarse-grained sediment waves in turbidity current channels and channel–lobe transition zones: Marine Geology, v. 192, p. 59–78.

Yagishita, K., 1994, Antidunes and traction-carpet deposits in deep-water channel sandstones, Cretaceous, British Columbia, Canada: Journal of Sedimentary Research, v. 64, p. 34–41.

Yang, T., Yingchang, C., and Yanzhong, W., 2017, A new discovery of the Early Cretaceous supercritical hyperpycnal flow deposits on Lingshan Island, East China: Acta Geologica Sinica, v. 91, p. 749–750.

Yih, C.S., and Guda, C.R., 1955, Hydraulic jump in a fluid system of two layers: Tellus, v. 7, p. 358–365.

Yokokawa, M., Hasegawa, K., Kanbayashi, S., and Endo, N., 2010, Formative conditions and sedimentary structures of sandy 3D antidunes: an application of the gravel step-pool model to fine-grained sand in an experimental flume: Earth Surface Processes Landforms, v. 35, p. 1720–1729.

Received 28 March 2018; accepted 19 February 2019.

Queries for sedp-89-06-02

This manuscript/text has been typeset from the submitted material. Please check this proof carefully to make sure there have been no font conversion errors or inadvertent formatting errors. Allen Press.